(MM) calculation, including the coordination and minimization of hydrogen and mutated side chain atoms, were performed with parm99SB and GLYCAM_06 force fields using the Amber program [61]. In detail, the system was at first minimized in an implicit water solvent using the Generalized Born (GB) model with force constant of 500 kcal/mol·Å$^2$ applied to all atoms except for mutated amino acids, followed by all atom minimization in the GB environment. Such modeled geometry for HA portion of 2009/H1N1pdm complex was confirmed to be similar to published PDB crystal structure of free HA [17] (RMSD of backbone atoms in HA1 was 154 Å). Using these geometries, the *ab initio* FMO calculations [36, 37, 62] were carried out under gas-phase conditions at the Hartree-Fock (HF) and Møller-Plesset second order (MP2) levels with the 6-31G* basis set [63,64]. Additionally, the FMO calculations using the spin-component scaled MP2 (SCS-MP2) methods [65, 66] were also carried out in order to modify the overestimation of MP2 binding energies. Note that the geometries of free HA and receptor were fixed at the complexed geometries in the binding energy calculations. The fragmentation of the system was as follows: each amino acid residue of HA, the sialic acid moiety, and each sugar moiety were treated as a single fragment (See Fig. (**2**)) [67]. Therefore, inter-fragment interaction energy (IFIE) analysis can be performed in an amino acid and sugar residue unit. All the FMO calculations were performed with the ABINIT-MP program, and the visualization was carried out with a BioStation Viewer [68]. In the following section, we discuss the results calculated at the FMO-MP2/6-31G* level of theory, unless otherwise stated.

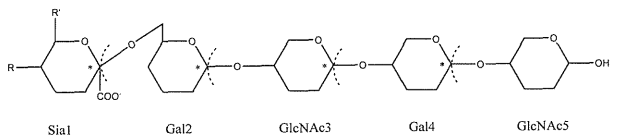


**Figure 2.** Schematic draw of fragmentation for the sialo-sugar chain. The '*' symbols indicate bond detached atom (BDA).

## 3. RESULTS

### 3.1. Binding Energies Between HA and Receptor

In order to estimate binding strength between HA and receptor, both binding energies and IFIEs were analyzed. The binding energies between HA and receptors were calculated by the following equation:

$$\bar{A}E = E(complex) - \{E(HA) + E(receptor)\} \quad (1)$$

where E(complex), E(HA), and E(receptor) were the total energy of HA-receptor complex, free HA, and free receptor, respectively. As shown in Fig. (**3a**), the overall structures among three HAs of 1930-swine, 2009/H1N1pdm, and 1934 human, were very similar. The calculated binding energies for these HAs were -234, -284, and -155 kcal/mol, respectively at the MP2/6-31G* level (Table **1**), indicating the strongest receptor binding for 2009/H1N1pdm. The SCS-MP2 treatment reduced the overestimation of correlation energies by almost 20%. The sum of IFIE between fragments of HA and those of receptor (IFIE sum) could also be used as the approximate estimation of binding energies [41,44]. Note that similar tendency was observed for IFIE sum values: IFIE sum between HA and receptor with three sugar chains were -263, -329, and -205 kcal/mol for 1930-swine, 2009/H1N1pdm, and 1934-human complexes, respectively (MP2/6-31G*).

### 3.2. 1930-Swine HA and 2009/H1N1pdm HA

Interactions between sialo-sugar chain and each amino acid residue of HA were compared between 1930-swine HA and 2009/H1N1pdm HA, based on the IFIE analysis. Fig. (**4**) shows numerical representations of IFIE for each residue of HAs with the five sialo-sugar chains receptor, Sia1-Gal2-GlcNAc3-Gal4-GlcNAc5. Residues with strong interactions such as Lys133 – Ala138 and Arg220 – Arg229 were located around the receptor. Some distant residues with negative charge (Asp and Glu) also indicated strong repulsive interactions (Fig. (**4a** and **4b**)). The IFIE results of 2009/ H1N1pdm were also visualized according to color in Fig. (**3e**). Fig. (**4c**) shows the IFIE difference between two HAs, ΔIFIE, and amino acids with the large absolute values of ΔIFIE are also listed in Table **2**. The residue 145 was remarkably stabilized for 2009/H1N1pdm HA with the Ser145Lys substitution (ΔIFIE = 97.4 kcal/mol). The molecular structure at the receptor binding site indicated that the sialic acid form an ionic pair with mutated Lys145 in addition to the hydrogen bond with Gln226 in the 2009/ H1N1pdm HA complex. Their distances were 1.79 and 2.10 Å, respectively (Fig. (**3c**)). For the 1930-swine HA, however, only the hydrogen bond with the Gln226 was observed (1.94 Å), and the Ser 145 was located at the distant position (3.54 Å) (Fig. (**3b**)). Such situation was thought to be a cause of large ΔIFIE value of Ser145Lys. Ala227Glu and Gly225Asp were also found to have large differences, -22.4 and -21.8 kcal/mol, respectively, which is located near the Gal2 moiety of the receptor. No other residue was observed around the receptor with the ΔIFIE of more than 10kcal/mol. Such small differences may originate in the molecular structure of 2009/H1N1pdm HA as a modeling structure from the 1930-swine HA template. As well as the binding energies, the individual IFIE values showed the same tendency among the MP2 and two SCS-MP2 methods.

### 3.3. 1934-Human HA and 2009/H1N1pdm HA

Interactions between the receptor and HA of both human H1N1 viruses, 2009/H1N1pdm and 1934-human, were also compared. Fig. (**5**) shows numerical representations of IFIE for each residue of HAs with the three sialo-sugar chains receptor, Sia1-Gal2-GlcNAc3. Binding energy of 2009/ H1N1pdm HA with the five sialo-sugar chains receptor was twice larger than that of 1934-human HA with the three sialo-sugar chains receptor (Table **1**). Different lengths of the sugar chains were thought to be one reason of such large difference. Here, interaction analysis with three sialo-sugar chain length of receptor was possible for both HAs based on the IFIE analysis. For the 2009/H1N1pdm, HA-receptor interactions were found to be similar to the case of five sialo-sugar chain receptor. For the 1934-human, residues strongly interacting with the sialo-sugar chain were similar to those of 2009/H1N1pdm, however, some repulsive residues, for instance Glu190, Glu219, Glu142 and Glu156, which were

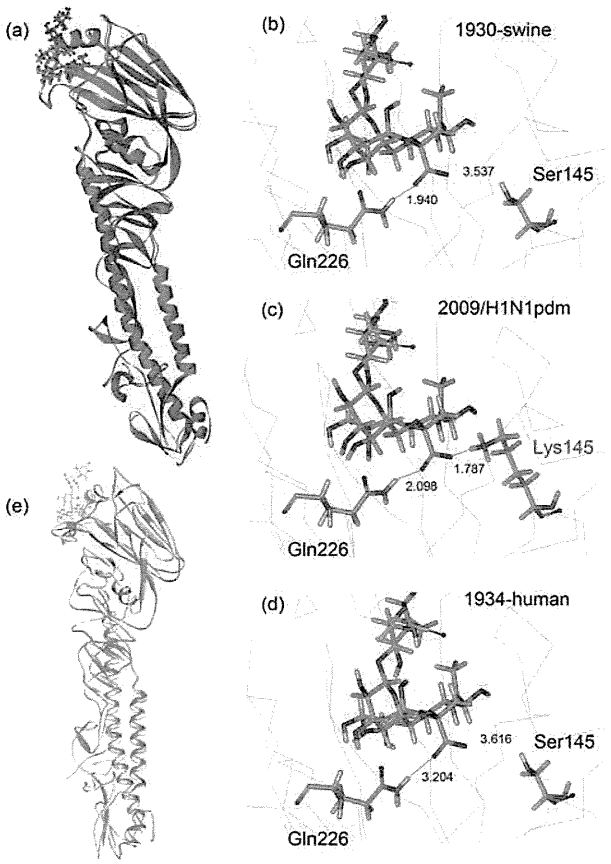


**Figure 3.** Molecular structures of three HAs (**a-d**). (**a**) Overall structures of superimposed backbones. (**b-d**) Structures at the sialo-sugar chain receptor binding site: (**b**) 1930-swine, (**c**) 2009/ H1N1pdm, and (**d**) 1934-human. Receptor, Gln226, and Lys145 (Ser145) are displayed with stick representation. The line representation is the Cα backbone. (**e**) Visualized IFIE results calculated at the MP2/6-31G* level for the complex for the 2009/H1N1pdm HA with α2-6 receptor (yellow). Red and blue for residues refer to the interaction energies of stabilization (negative) and destabilization (positive), respectively. The range from -20 to +20 kcal/mol is shown with gradation.

**Table 1. Binding Energies and Inter Fragment Interaction Energy (IFIE) Between HA and Receptor**

| | | 1930-Swine | 2009/H1N1pdm | 1934-Human |
|---|---|---|---|---|
| HF/6-31G* | ΔE | -172.5[a] | -217.8[a] | -106.0[b] |
| | IFIE[a] | -217.6 | -273.4 | - |
| | IFIE[b] | -198.3 | -256.1 | -145.5 |
| MP2/6-31G* | ΔE | -234.4[a] | -284.2[a] | -154.7[b] |
| | IFIE[a] | -291.7 | -353.9 | - |
| | IFIE[b] | -263.1 | -328.7 | -204.8 |
| SCS-MP2 (Grimme) | ΔE | -219.9[a] | -268.7[a] | -143.2[b] |
| | IFIE[a] | -276.5 | -337.5 | - |
| | IFIE[b] | -249.8 | -313.8 | -192.8 |
| SCS-MP2 (Hill) | ΔE | -227.0[a] | -276.3[a] | -149.1[b] |
| | IFIE[a] | -278.5 | -339.6 | - |
| | IFIE[b] | -251.6 | -315.9 | -193.9 |

in kcal/mol
a Sia1-Gal2-GlcNAc3-Gal4-GlcNAc5 was used as the receptor
b Sia1-Gal2-GlcNAc3 was used as the receptor

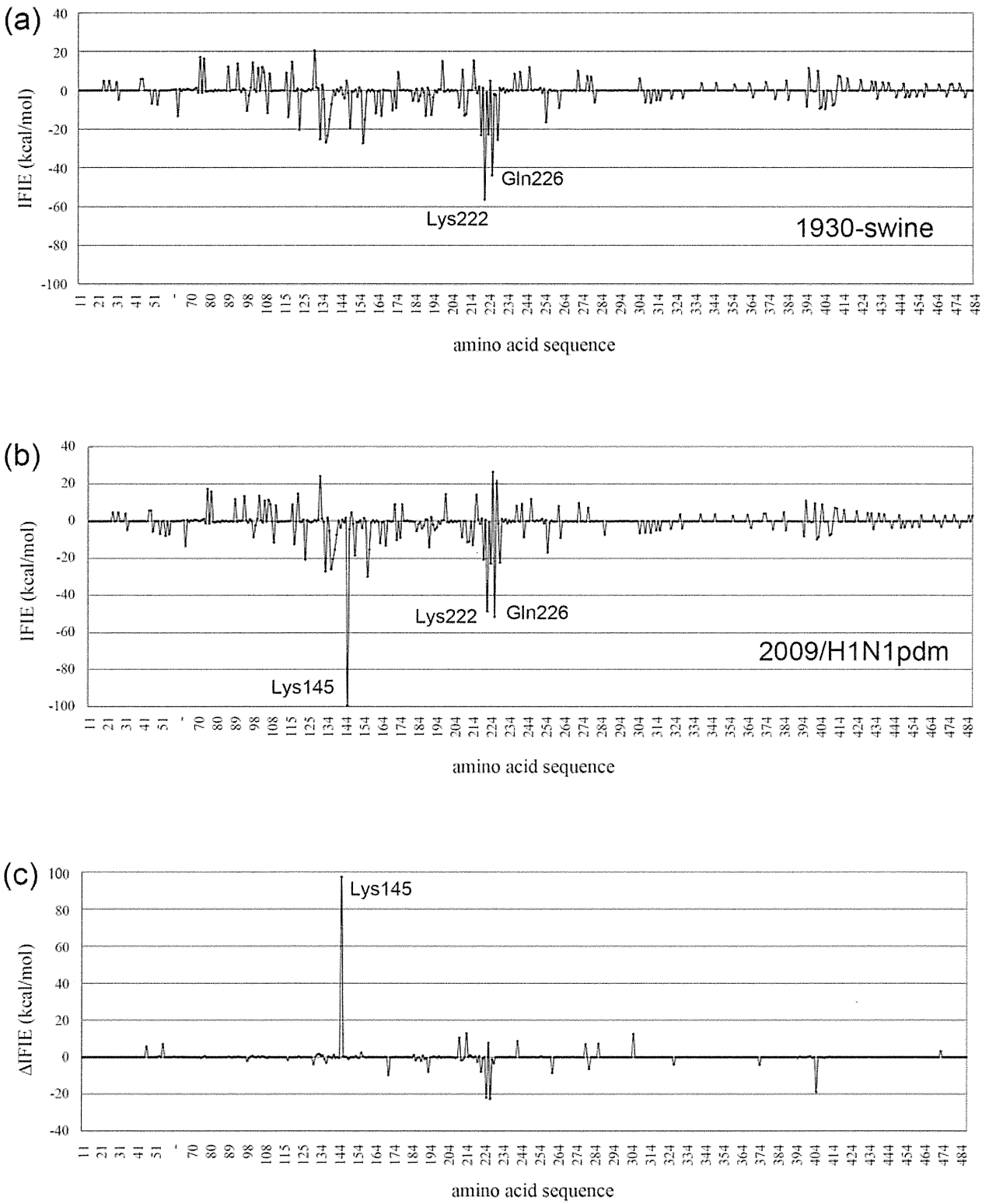


**Figure 4.** IFIEs between the five sialo-sugar chains receptor and each amino acid residue fragment of HAs: (**a**) 1930-swine, (**b**) 2009/H1N1pdm, and (**c**) their differences (**a-b**).

**Table 2. IFIEs Between Five Sialo-Sugar Chains Receptor and each Amino Acid Residue of the HAs**

| 1930-swine | | 2009/H1N1pdm | | |
|---|---|---|---|---|
| **Residue** | **IFIE** | **Residue** | **IFIE** | **ΔIFIE** |
| Ser145 | -2.08 | Lys145 | -99.46 | 97.4 |
| Thr214 | 0.16 | Lys214 | -12.77 | 12.9 |
| Glu305 | 6.20 | Lys305 | -6.39 | 12.6 |
| Asp210 | 10.59 | Ser210 | 0.05 | 10.5 |
| Thr242 | 0.13 | Lys242 | -8.66 | 8.8 |
| Gln226 | -43.92 | Gln226 | -51.66 | 7.7 |
| His286 | 0.03 | Lys286 | -7.27 | 7.3 |
| Gly60 | 0.12 | Arg60 | -6.99 | 7.1 |
| Asp279 | 7.10 | Asn279 | 0.12 | 7.0 |
| Ser46 | 0.09 | Lys46 | -5.63 | 5.7 |
| Lys281 | -6.16 | Thr281 | 0.09 | -6.2 |
| Lys222 | -56.56 | Lys222 | -48.72 | -7.8 |
| Ser193 | -12.62 | Ser193 | -4.70 | -7.9 |
| Asn261 | -0.34 | Glu261 | 8.19 | -8.5 |
| Asn171 | -0.44 | Asp171 | 9.17 | -9.6 |
| Lys405 | -9.66 | Glu405 | 9.14 | -18.8 |
| Gly225 | 4.94 | Asp225 | 26.76 | -21.8 |
| Ala227 | -1.97 | Glu227 | 20.48 | -22.4 |

substituted residues, were newly observed. ΔIFIE values in Fig. (**5c**) and Table **3** show, again, a high peak at position 145, where different residues were observed between 2009/ H1N1pdm and 1934-human HAs (ΔIFIE = 100.9 kcal/mol). Also, IFIE at the Gln226 was destabilized for 1934-human, ΔIFIE = 25.9 kcal/mol. This is because the hydrogen bond length between sialic acid and Gln226 was observed to be longer (3.20 Å) than 2009/H1N1pdm (Fig. (**3d**)). The other hydrogen bond length of sialic acid with the Ser145 was still long (3.62 Å). Another large ΔIFIE values were observed at the positions where different amino acid residues were found between 1934-human and 2009/H1N1pdm HAs. Compared to the difference between 1930-swine and 2009/H1N1pdm HAs, larger ΔIFIEs (more than 10kcal/mol) were monitored at extensive positions of 2009/H1N1pdm and 1934-human HA.

## 4. DISCUSSION

Summarizing three HAs, both amino acid sequence and overall backbone structures were very similar (Fig. (**1** and **3a**)). The amino acid sequence of receptor binding site, Helix190 (190-198), Loop130 (135-138), Loop220 (221-228), Tyr98, Trp153, and His183 [38], were highly conserved. However, the side chain structures at the receptor binding site (Fig. (**3b-3d**)) indicated that the sialic acid formed hydrogen bond with the Gln226 for all three HAs but an additional ionic pair bond between residue Lys145 and the sialic acid was found only for 2009/H1N1pdm HA. Both 1930-swine and 1934-human HAs have Ser145, which formed a weak or no hydrogen bond with the sialic acid. Most of 2009/ H1N1pdm HA has Lys at the position 145. IFIE analysis provided quantitative theoretical evidence for these interactions, and such hydrogen bonds and ionic pair networks made strong bindings between 2009/H1N1pdm HA and human-type receptor. Therefore, the current swine-origin pandemic virus has been found to recognize the α2-6 receptors (human type) much stronger than 1934-human, a prototype human virus, and 1930-swine, an ancestor of the 2009/ H1N1pdm virus.

Furthermore, together with the discussions based on the steric structures [5], IFIE analysis provides in-depth information about HA-receptor interaction. Sum of IFIE values between α2-6 receptor (three sialo-sugar chain length) and a positively charged 'lysine fence'-which are constructed from Lys133, Lys145, and Lys222 in 2009/H1N1pdm (Cal4); from Arg133, Ser145, and Lys222 in 1930-swine; and from gap at position 133 (see Fig. (**1**)), Ser145, and Lys222 in 1934-human-were -184.7, -89.0, and -60.4 kcal/mol, respectively. Clearly, interactions between such 'lysine fence' of 2009/H1N1pdm and α2-6 receptor stabilize their binding.

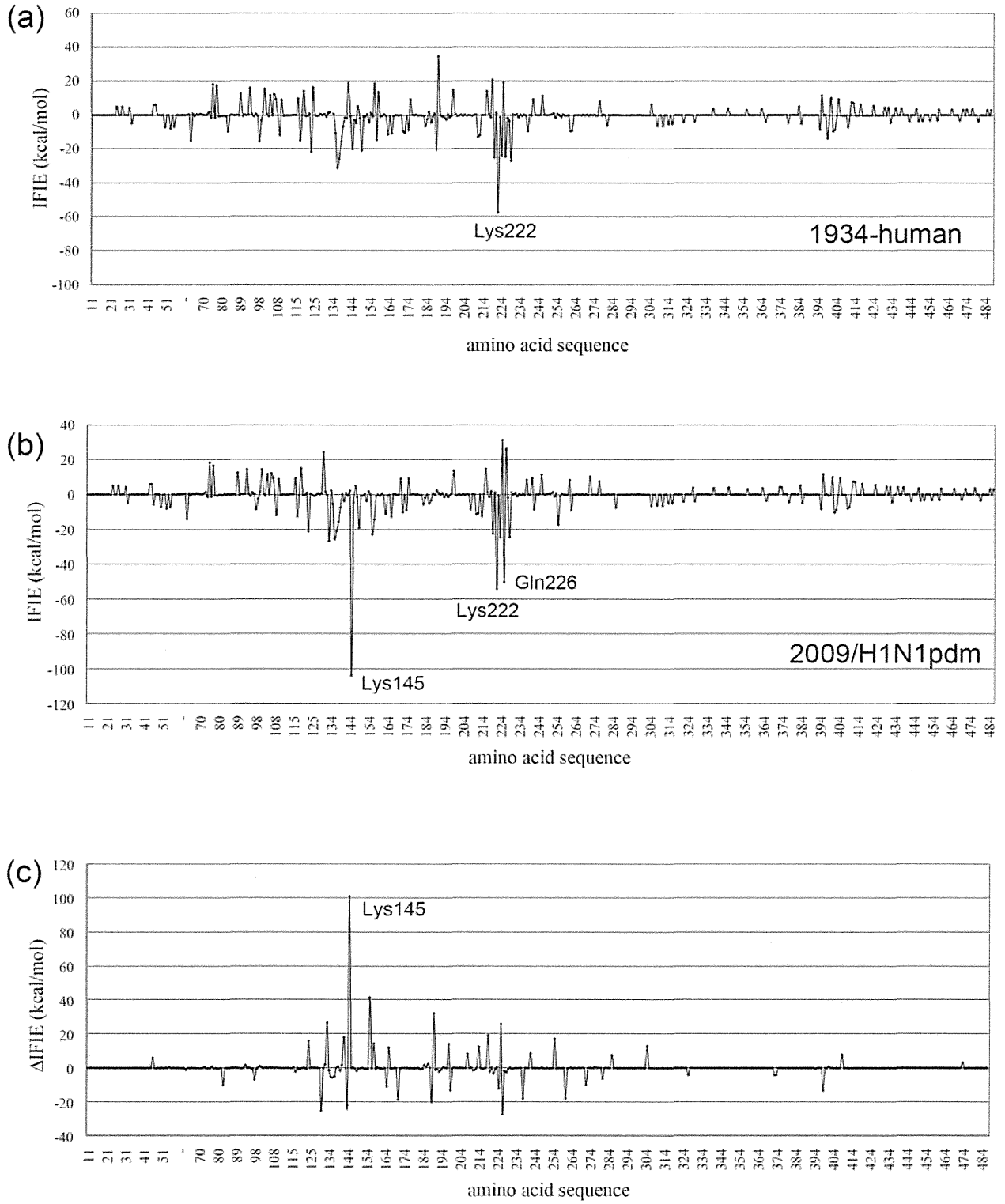


**Figure 5.** IFIEs between the three sialo-sugar chains receptor and each amino acid residue fragment of HAs: (**a**) 1934-human, (**b**) 2009/H1N1pdm, and (**c**) their differences (**a-b**).

**Table 3. IFIEs Between Three Sialo-Sugar Chains Receptor and each Amino Acid Residue of the HAs**

| 1934-Human | | 2009/H1N1pdm | | |
|---|---|---|---|---|
| **Residue** | **IFIE** | **Residue** | **IFIE** | **ΔIFIE** |
| Ser145 | -2.88 | Lys145 | -103.82 | 100.9 |
| Glu156 | 18.80 | Lys156 | -22.80 | 41.6 |
| Glu190 | 34.82 | Asp190 | 2.51 | 32.3 |
| Gln226 | -24.49 | Gln226 | -50.37 | 25.9 |
| Glu219 | 20.83 | Ile219 | 1.71 | 19.1 |
| Glu142 | 18.90 | Ala142 | 0.86 | 18.0 |
| Met255 | -0.02 | Arg255 | -17.18 | 17.2 |
| Glu124 | 16.23 | Thr124 | 0.46 | 15.8 |
| Glu158 | 13.49 | Gly158 | -0.87 | 14.4 |
| Glu198 | 14.81 | Ala198 | 0.71 | 14.1 |
| Glu305 | 6.46 | Lys305 | -6.54 | 13.0 |
| Thr214 | 0.01 | Lys214 | -12.45 | 12.5 |
| Asn166 | -0.78 | Lys166 | -12.87 | 12.1 |
| Arg82 | -9.74 | Ser82 | 0.37 | -10.1 |
| Asn272 | 0.20 | Asp272 | 10.33 | -10.1 |
| Lys165 | -10.86 | Ser165 | -0.14 | -10.7 |
| Asp225 | 19.10 | Asp225 | 31.18 | -12.1 |
| Asn199 | 0.55 | Asp199 | 13.59 | -13.0 |
| Lys399 | -13.78 | His399 | -0.55 | -13.2 |
| Arg261 | -9.52 | Glu261 | 8.30 | -17.8 |
| Lys238 | -9.57 | Glu238 | 8.37 | -17.9 |
| Lys171 | -9.41 | Asp171 | 9.18 | -18.6 |
| Lys189 | -19.99 | Ala189 | -0.16 | -19.8 |
| Lys144 | -20.03 | Ala144 | 2.02 | -22.1 |
| Asn(130+1) | -0.90 | Asp(130+1) | 24.15 | -25.1 |
| Ala227 | -1.74 | Glu227 | 25.66 | -27.4 |

However, additional contact of 2009/H1N1pdm with α2-6 receptor by Asp225 destabilizes their binding; IFIE between α2-6 receptor and Asp225 (2009/H1N1pdm), Gly225 (1930-swine), and Asp225 (1934-human) were 31.2, 19.1, and 5.1 kcal/mol, respectively (See Table **S2** for detailed IFIE values). Such repulsive interaction may not exist for the complex between 2009/H1N1pdm and α2-3 receptor [5], which may cause their greater affinity.

## 5. CONCLUSION

In terms of the quantum mechanical FMO analysis, we have quantitatively analyzed the binding affinity of HAs (2009/H1N1pdm, 1930-swine, and 1934-human) to α2-6 receptors, as analogs of human receptors. Through the IFIE analysis based on the FMO calculations, we could also specify and characterize important residues which would play an essential role in the binding specificity between HA and a receptor; especially the Lys145 was found to be an important characteristic of the 2009 pandemic virus HA.

## ACKNOWLEDGMENTS

The authors thank Prof. Yuji Mochizuki, Dr. Tatsuya Nakano, and Mr. Kazutomo Takematsu for discussions about FMO calculations. The authors also thank Mr. Katsumi Yamashita, Dr. Yoshio Okiyama, and Mr. Akifumi Kato for development of ABINIT-MP and BioStation Viewer codes. This work was primarily supported by the "Core Research for Evolutional Science and Technology" project of the Ja-

pan Science and Technology Agency (JST-CREST). A part of this research was also carried out in conjunction with the "Research and Development of Innovative Simulation Software (RISS)" project supported by the Ministry of Education, Culture, Sports, Science, and Technology (MEXT).

## SUPPLEMENTARY MATERIAL

Supplementary material is available on the publishers Web site along with the published article.

## REFERENCES

[1] Neumann, G.; Noda, T.; Kawaoka, Y. Emergence and pandemic potential of swine-origin H1N1 influenza virus. *Nature*, **2009**, *459*, 931-939.

[2] Smith, G. J. D.; Vijaykrishna, D.; Bahl, J.; Lycett, S. J.; Worobey, M.; Pybus, O. G.; Ma, S. K.; Cheung, C. L.; Raghwani, J.; Bhatt, S.; Malik Peiris, J. S.; Guan, Y.; Rambaut, A. Origins and evolutionary genomics of the 2009 swine-origin H1N1 influenza A epidemic. *Nature*, **2009**, *459*, 1122-1126.

[3] Garten, R. J.; Davis, C. T.; Russell, C. A.; Shu, B.; Lindstrom, S.; Balish, A.; Sessions, W. M.; Xu, X.; Skepner, E.; Deyde, V.; Okomo-Adhiambo, M.; Gubareva, L.; Barnes, J.; Smith, C. B.; Emery, S. L.; Hillman, M. J.; Rivailler, P.; Smagala, J.; de Graaf, M.; Burke, D. F.; Fouchier, R. A. M.; Pappas, C.; Alpuche-Aranda, C. M.; López-Gatell, H.; Olivera, H.; López, I.; Myers, C. A.; Faix, D.; Blair, P. J.; Yu, C.; Keene, K. M.; Dotson Jr., P. D.; Boxrud, D.; Sambol, A. R.; Abid, S. H.; St. George, K.; Bannerman, T.; Moore, A. L.; Stringer, D. J.; Blevins, P.; Demmler-Harrison, G. J.; Ginsberg, M.; Kriner, P.; Waterman, S.; Smole, S.; Guevara, H. F.; Belongia, E. A.; Clark, P. A.; Beatrice, S. T.; Donis, R.; Katz, J.; Finelli, L.; Bridges, C. B.; Shaw, M.; Jernigan, D. B.; Uyeki, T. M.; Smith, D. J.; Klimov, A. I.; Cox, N. J. Antigenic and genetic characteristics of swine-origin 2009 A(H1N1) influenza viruses circulating in humans. *Science*, **2009**, *325*, 197-201.

[4] Schnitzler, S. U.; Schnitzler, P. An update on swine-origin influenza virus A/H1N1: a review. *Virus Genes*, **2009**, *39*, 279-292.

[5] Soundararajan, V.; Tharakaraman, K.; Raman, R.; Raguram, S.; Shriver, Z.; Sasisekharan, V.; Sasisekharan, R. Extrapolating from sequence—the 2009 H1N1 'swine' influenza virus. *Nat. Biotech.*, **2009**, *27*, 510-513.

[6] Ito, T.; Couceiro, J. N. S. S.; Kelm, S; Baum, L. G.; Krauss, S.; Castrucci, M. R.; Donatelli, I.; Kida, H.; Paulson, J. C.; Webster, R. G.; Kawaoka Y. Molecular basis for the generation in pigs of influenza a viruses with pandemic potential. *J. Virol.*, **1998**, *72*, 7367-7373.

[7] Skehel, J. J.; Wiley, D.C. Receptor binding and membrane fusion in virus entry: the influenza hemagglutinin. *Ann. Rev. Biochem.*, **2000**, *69*, 531-569.

[8] Horimoto, T.; Kawaoka, Y. Influenza: lessons from past pandemics, warnings from current incidents, *Nat. Rev. Microbiol.*, **2005**, *3*, 591-600.

[9] Neumann, G.; Kawaoka, Y. Host range restriction and pathogenicity in the context of influenza pandemic. *Emerg. Infect. Dis.*, **2006**, *12*, 881-886.

[10] Pielak, R. M.; Chou, J. J. Influenza M2 proton channels. *Biochim. Biophys. Acta*, **2010**, 10.1016/j.bbamem.2010.1004.1015.

[11] Suzuki, Y. Sialobiology of influenza: molecular mechanism of host range variation of influenza viruses. *Biol. Pharm. Bull.*, **2005**, *28*, 399-408.

[12] Du, Q. S.; Wang, S. Q.; Huang, R. B.; Chou, K. C. Computational 3D structures of drug-targeting proteins in the 2009-H1N1influenza A virus. *Chem. Phys. Lett.*, **2010**, *485*, 191-195.

[13] Wang, J. F.; Chou, K. C. Insights from studying the mutation-induced allostery in the M2 proton channel by molecular dynamics. *Protein Eng Des Sel.*, **2010**, *23*, 663-666.

[14] Wang, J. F.; Wei, D. Q.; Chou, K. C. Insights from investigating the interactions of adamantane-based drugs with the M2 proton channel from the H1N1 swine virus. *Biochem. Biophys. Res. Commun.*, **2009**, *388*, 413-417.

[15] Wang, S. Q.; Du, Q. S.; Huang, R. B.; Zhang, D. W.; Chou, K. C. Insights from investigating the interaction of oseltamivir (Tamiflu) with neuraminidase of the 2009 H1N1 swine flu virus. *Biochem. Biophys. Res. Commun.* **2009**, *386*, 432-436.

[16] NCBI. Influenza Virus Resource. http://www.ncbi.nlm.nih.gov/genomes/FLU/FLU.html

[17] Xu, R.; Ekiert, D. C.; Krause, J. C.; Hai, R.; Crowe Jr., J. E.; Wilson I. A. Structural Basis of Preexisting Immunity to the 2009 H1N1 Pandemic Influenza Virus. *Science*, **2010**, *328*, 357-360.

[18] Gamblin, S. J.; Haire, L. F.; Russell, R. J.; Stevens, D. J.; Xiao, B.; Ha, Y.; Vasisht, N.; Steinhauer, D. A.; Daniels, R. S.; Elliot, A.; Wiley, D. C.; Skehel J. J. The structure and receptor binding properties of the 1918 influenza hemagglutinin. *Science*, **2004**, *303*, 1838-1842.

[19] Schnell, J. R.; Chou, J. J. Structure and mechanism of the M2 proton channel of influenza A virus. *Nature*, **2008**, *451*, 591-595.

[20] Pielak, R. M.; Jason R. Schnell, J. R.; Chou, J. J. Mechanism of drug inhibition and drug resistance of influenza A M2 channel. *Proc. Natl. Acad. Sci. USA*, **2009**, *106*, 7379-7384.

[21] Wang, J.; Pielak, R. M.; McClintock, M. A.; Chou, J. J. Solution structure and functional analysis of the influenza B proton channel. *Nat. Struct. Mol. Biol.*, **2009**, *16*, 1267-1271.

[22] Pielak, R. M.; Chou, J. J. Solution NMR structure of the V27A drug resistant mutant of influenza A M2 channel. *Biochem. Biophys. Res. Commun.*, **2010**, *401*, 58-63.

[23] Pielak, R. M.; Chou, J. J. Flu channel drug resistance: a tale of two sites. *Protein Cell*, **2010**, *1*, 246-258.

[24] Huang, R. B.; Du, Q. S.; Wang, C. H.; Chou, K. C. An in-depth analysis of the biological functional studies based on the NMR M2 channel structure of influenza A virus. *Biochem. Biophys. Res. Comm.*, **2008**, *377*, 1243-1247.

[25] Du, Q. S.; Huang, R. B.; Wang, C. H.; Li, X. M.; Chou, K. C. Energetic analysis of the two controversial drug binding sites of the M2 proton channel in influenza A virus. *J. Theor. Biol.*, **2009**, *259*, 159-164.

[26] Wei, H.; Wang, C. H.; Du, Q. S.; Meng, J.; Chou, K. C. Investigation into adamantane-based M2 inhibitors with FB-QSAR. *Med. Chem.*, **2009**, *5*, 305-317.

[27] Wang, N. X.; Zheng, J. J. Computational studies of H5N1 influenza virus resistance to oseltamivir. *Protein Sci.*, **2009**, *18*, 707-715.

[28] Wei, D. Q.; Du, Q. S.; Sun, H.; Chou, K. C. Insights from modeling the 3D structure of H5N1 influenza virus neuraminidase and its binding interactions with ligands. *Biochem. Biophys. Res. Comm.*, **2006**, *344*, 1048-1055.

[29] Wang, S. Q.; Du, Q. S.; Chou, K. C. Study of drug resistance of chicken influenza A virus (H5N1) from homology-modeled 3D structures of neuraminidases. *Biochem. Biophys. Res. Comm.*, **2007**, *354*, 634-640.

[30] Du, Q. S.; Wang, S. Q.; Chou, K. C. Analogue inhibitors by modifying oseltamivir based on the crystal neuraminidase structure for treating drug-resistant H5N1 virus. *Biochem. Biophys. Res. Comm.*, **2007**, *362*, 525-531.

[31] Gong, K.; Li, L.; Wang, J. F.; Cheng, F.; Wei, D. Q.; Chou, K. C. Binding mechanism of H5N1 influenza virus neuraminidase with ligands and its implication for drug design. *Med. Chem.*, **2009**, *5*, 242-249.

[32] Du, Q. S.; Huang, R. B.; Wang, S. Q.; Chou, K. C. Designing inhibitors of M2 proton channel against H1N1 swine influenza virus. *PLoS One*, **2010**, *5*, e9388.

[33] Du, Q. S.; Huang, R. B.; Wang, C. H.; Li, X. M.; Chou, K. C. Energetic analysis of the two controversial drug binding sites of the M2 proton channel in influenza A virus. *J. Theor. Biol.*, **2009**, *259*, 159-164.

[34] Wei, H.; Wang, C. H.; Du, Q. S.; Meng, J.; Chou, K. C. Investigation into adamantane-based M2 inhibitors with FB-QSAR. *Med. Chem.*, **2009**, *5*, 305-317.

[35] Wang, S. Q.; Cheng, X. C.; Dong, W. L.; Wang, R. L.; Chou, K. C. Three new powerful Oseltamivir derivatives for inhibiting the neuraminidase of influenza virus. *Biochem. Biophys. Res. Commun.*, **2010**, *401*, 188-191.

[36] Fedorov, D. G.; Kitaura, K. Eds.; The Fragment Molecular Orbital Method: Practical Applications to Large Molecular Systems; CRC Press: Boca Raton, FL, **2009**.

[37] Fedorov, D.G.; Kitaura, K. Extending the Power of Quantum Chemistry to Large Systems with the Fragment Molecular Orbital Method. *J. Phys. Chem.*, **2007**, *A 111*, 6904-6914.

[38] Iwata, T.; Fukuzawa, K.; Nakajima, K.; Aida-Hyugaji, S.; Mochizuki, Y.; Watanabe, H.; Tanaka, S. Theoretical analysis of binding specificity of influenza viral hemagglutinin to avian and human receptors based on the fragment molecular orbital method Comp. *Biol. Chem.*, **2008**, *32*, 198-211.

[39] Sawada, T.; Hashimoto, T., Nakano, H.; Suzuki, T.; Ishida, H.; Kiso, M. Why does avian influenza A virus hemagglutinin bind to avian receptor stronger than to human receptor? Ab initio fragment molecular orbital studies. *Biochem. Biophys. Res. Comm.*, **2006**, *351*, 40-43.

[40] Sawada, T.; Hashimoto, T.; Tokiwa, H.; Suzuki, T.; Nakano, H.; Ishida, H.; Kiso, M.; Suzuki, Y. Ab initio fragment molecular orbital studies of influenza virus hemagglutinin–sialosaccharide complexes toward chemical clarification about the virus host range determination. *Glycoconj. J.*, **2008**, *25*, 805-815.

[41] Takematsu, K.; Fukuzawa, K.; Omagari, K.; Nakajima, S.; Nakajima, K.; Mochizuki, Y.; Nakano, T.; Watanabe, H.; Tanaka, S. Possibility of Mutation Prediction of Influenza Hemagglutinin by Combination of Hemadsorption Experiment and Ab Initio Calculation for Antibody Binding. *J. Phys. Chem.*, **2009**, *B 113*, 4991-4994.

[42] Mochizuki, Y.; Yamashita, K.; Murase, T.; Nakano, T.; Fukuzawa, K.; Takematsu, K.; Watanabe, H.; Tanaka, S. Large scale FMO-MP2 calculations on a massively parallel-vector computer. *Chem. Phys. Lett.*, **2008**, *457*, 396-403.

[43] Mochizuki, Y.; Yamashita, K.; Fukuzawa, K.; Takematsu, K.; Watanabe, H.; Taguchi, N.; Okiyama, Y.; Tsuboi, M.; Nakano, T.; Tanaka, S. Large-scale FMO-MP3 calculations on the surface proteins of influenza virus, hemagglutinin (HA) and neuraminidase (NA). *Chem. Phys. Lett.*, **2010**, *493*, 346-352.

[44] Fukuzawa, K.; Mochizuki, Y.; Tanaka, S.; Kitaura, K.; Nakano, T. Molecular Interactions between Estrogen Receptor and Its Ligand Studied by the Ab Initio Fragment Molecular Orbital Method. *J. Phys. Chem. B*, **2006**, *110*, 16102-16110; *ibid.*, **2006**, *110*, 24276-24276.

[45] Chou, K. C. Review: Structural bioinformatics and its impact to biomedical science. *Curr. Med. Chem.*, **2004**. *11*. 2105-2134.

[46] Chou, K. C. Modelling extracellular domains of GABA-A receptors: subtypes 1, 2, 3, and 5. *Biochem. Biophys. Res. Commun.*, **2004**, *316*, 636-642.

[47] Chou, K. C. Molecular therapeutic target for type-2 diabetes. *J. Proteome Res.*, **2004**, *3*, 1284-1288.

[48] Ban, H. S.; Usui, T.; Nabeyama, W.; Morita, H.; Fukuzawa, K.; Nakamura, H. Discovery of Boron-conjugated 4-Anilinoquinazoline as a Prolonged Inhibitor of EGFR Tyrosine Kinase. *Org. Biomol. Chem.*, **2009**, *7*, 4415-4427.

[49] Chou, K. C.; Wei, D. Q.; Zhong, W. Z. Binding mechanism of coronavirus main proteinase with ligands and its implication to drug design against SARS. (Erratum: ibid., 2003, Vol.310, 675). *Biochem. Biophys. Res. Comm.*, **2003**, *308*, 148-151.

[50] He, Z. S.; Zhang, J.; Shi, X. H.; Hu, L. L.; Kong, X. G.; Cai, Y. D.; Chou, K. C. Predicting drug-target interaction networks based on functional groups and biological features. *PLoS One*, **2010**, 5, e9603.

[51] Chou, K. C.; Wei, D. Q.; Du, Q. S.; Sirois, S.; Zhong, W. Z. Review: Progress in computational approach to drug development against SARS. *Curr. Med. Chem.*, **2006**, *13*, 3263-3270.

[52] Chou, K. C. Energy-optimized structure of antifreeze protein and its binding mechanism. *J. Mol. Biol.*, **1992**, *223*, 509-517.

[53] Chou, K. C.; Jones, D.; Heinrikson, R. L. Prediction of the tertiary structure and substrate binding site of caspase-8. *FEBS Lett.*, **1997**, *419*, 49-54.

[54] Chou, K. C. Coupling interaction between thromboxane A2 receptor and alpha-13 subunit of guanine nucleotide-binding protein. *J Proteome Res.*, **2005**, *4*, 1681-1686.

[55] Wang, J. F.; Wei, D. Q.; Li, L.; Zheng, S. Y.; Li, Y. X.; Chou, K. C. 3D structure modeling of cytochrome P450 2C19 and its implication for personalized drug design. *Biochem. Biophys. Re.s Commun.*, (Corrigendum: ibid, 2007, Vol. 357, 330), **2007**, *355*, 513-519.

[56] Li, L.; Wei, D. Q.; Wang, J. F.; Chou, K. C. Computational studies of the binding mechanism of calmodulin with chrysin. *Biochem. Biophys. Res. Comm.*, **2007**, *358*, 1102-1107.

[57] Wang, J. F.; Wei, D. Q.; Lin, Y.; Wang, Y. H.; Du, H. L.; Li, Y. X.; Chou, K. C. Insights from modeling the 3D structure of NAD(P)H-dependent D-xylose reductase of Pichia stipitis and its binding interactions with NAD and NADP. *Biochem. Biophys. Res. Comm.*, **2007**, *359*, 323-329.

[58] Gu, R. X.; Gu, H.; Xie, Z. Y.; Wang, J. F.; Arias, H. R.; Wei, D. Q.; Chou, K. C. Possible drug candidates for Alzheimer's disease deduced from studying their binding interactions with alpha7 nicotinic acetylcholine receptor. *Med. Chem.*, **2009**, 5, 250-262.

[59] Wang, J. F.; Yan, J. Y.; Wei, D. Q.; Chou, K. C. Binding of CYP2C9 with diverse drugs and its implications for metabolic mechanism. *Med. Chem.*, **2009**, *5*, 263-270.

[60] Wang, J. F.; Wei, D. Q.; Chen, C.; Li, Y.; Chou, K. C. Molecular modeling of two CYP2C19 SNPs and its implications for personalized drug design. *Protein Pept. Lett.*, **2008**, *15*, 27-32.

[61] Case, D. A.; Darden, T. A.; Cheatham, T. E.; Simmerling, III, C. L.; Wang, J.; Duke, R. E.; Luo, R.; Walker, R. C.; Zhang, W.; Merz, K. M.; Roberts, B. P.; Wang, B.; Hayik, S.; Roitberg, A.; Seabra, G.; Kolossváry, I.; Wong, K. F.; Paesani, F.; Vanicek, J.; Wu, X.; Brozell, S. R.; Steinbrecher, T.; Gohlke, H.; Cai, Q.; Ye, X.; Wang, J.; Hsieh, M.-J.; Cui, G.; Roe, D. R.; Mathews, D. H.; Seetin, M. G.; Sagui, C.; Babin, V.; Luchko, T.; Gusarov, S.; Kovalenko, A.; Kollman, P. A. AMBER 11. University of California: San Francisco, **2010**.

[62] Nakano, T.; Kaminuma, T.; Sato, T.; Fukuzawa, K.; Akiyama, Y.; Uebayasi, M.; Kitaura, K. Frgment Molecular Orbital Method: Use of Approximate Electrostatic Potential. *Chem. Phys. Lett.*, **2002**, *351*, 475-480.

[63] Mochizuki, Y.; Nakano, T.; Koikegami, S.; Tanimori, S.; Abe, Y.; Nagashima, U.; Kitaura, K. A parallelized integral-direct second-order Møller–Plesset perturbation theory method with a fragment molecular orbital scheme. *Theor. Chem. Acc.*, **2004**, *112*, 442-452.

[64] Mochizuki, Y.; Koikegami, S.; Nakano, T.; Amari, S.; Kitaura, K. Large scale MP2 calculations with fragment molecular orbital scheme. *Chem. Phys. Lett.*, **2004**, *396*, 473-479.

[65] Grimme, S. J. Improved second-order Møller–Plesset perturbation theory by separate scaling of parallel- and antiparallel-spin pair correlation energies. *Chem. Phys.*, **2003**, *118*, 9095-9102.

[66] Hill, J. G.; Platts, J. A. Spin-Component Scaling Methods for Weak and Stacking Interactions. *Phys. Chem. Chem. Phys.*, **2006**. *8*. 4072-4078.

[67] Sawada, T.; Fedorov, D. G.; Kitaura, K. Structural and Interaction Analysis of Helical Heparin Oligosaccharides with the Fragment Molecular Orbital Method. *Int. J. Quantum Chem.*, **2009**, *109*, 2033-2045.

[68] ABINIT-MP ver 4.3 and BioStation Viewer ver. 12.0 is available from the website of RSS21 project: http://www.ciss.iis.u-tokyo.ac.jp/dl.

[69] CLUSTALW version 1.83: http://clustalw.ddbj.nig.ac.jp

**Received: October 11, 2010** **Revised: December 16, 2010** **Accepted: December 18, 2010**

Bioorganic & Medicinal Chemistry Letters 22 (2012) 1251–1254

Contents lists available at SciVerse ScienceDirect

Bioorganic & Medicinal Chemistry Letters

journal homepage: www.elsevier.com/locate/bmcl

# Immobilization of fluorous oligosaccharide recognized by influenza virus on polytetrafluoroethylene filter

Mami Tojino [a], Masako Mori [a], Maria Carmelita Z. Kasuya [b], Kenichi Hatanaka [b], Atsushi Kawaguchi [c], Kyosuke Nagata [c], Takashi Shirai [a], Mamoru Mizuno [a,*]

[a] Laboratory of Glyco-organic Chemistry, The Noguchi Institute, 1-8-1 Kaga, Itabashi-ku, Tokyo 173-0003, Japan
[b] Institute of Industrial Science, The University of Tokyo, 4-6-1 Komaba, Meguro-ku, Tokyo 153-8505, Japan
[c] Department of Infection Biology, Faculty of medicine and Comprehensive Human Sciences, University of Tsukuba, 1-1-1 Tennodai, Tsukuba 305-8575, Japan

ARTICLE INFO

*Article history:*
Received 12 October 2011
Revised 2 November 2011
Accepted 9 November 2011
Available online 22 November 2011

*Keywords:*
Fluorous
Oligosaccharide
Saccharide primer
Polytetrafluoroethylene filter
Influenza virus

ABSTRACT

The lactoside with PEG-fluorous tag was introduced to BHK-21(C-13) cells to generate a GM3-type oligosaccharide (Siaα2-3Galβ1-4Glc). The GM3-type oligosaccharide obtained was easily immobilized by spotting onto commercially available polytetrafluoroethylene (PTFE) filter through non-covalent fluorous affinity and simply assessed by dot blot method using the interaction of carbohydrate- with proteins which recognize sialic acid such as virus membrane proteins.



Since the Curran group introduced the fluorous tag method, it has been widely employed to facilitate the separation of the products by fluorous solid-phase extraction (SPE), reverse fluorous SPE or liquid–liquid extraction.[1] Recently, different strategies using the fluorous tag was developed for application to carbohydrate and small molecule microarrays.[2,3] In these methods, the highly specific fluorous affinity interaction arises between the fluorous tagged compound and the fluoroalkyl modified glass surface. This fluorous affinity interaction differs from covalent binding interaction. The compounds for covalent immobilization require a chemically active group.[4] On the other hand, the compounds for the non-covalent fluorous immobilization do not require a specific active group, but a chemically inert fluorous tag that could facilitate separation and minimize the synthetic process by eliminating the protection step. However, a key issue for various immobilizations is production of the complex substrates. Recently, we reported the saccharide primer method using mouse melanoma B16 cells and lactoside or GlcNAc primer with fluorous tag.[5] It is known that the saccharide primer method using animal cells is simple and involves regio- and stereospecific glycosylation.[6] Using mouse melanoma B16 cells, a GM3-type oligosaccharide (Siaα2-3Galβ1-4Glc), which is capable of binding to highly pathogenic avian influenza viruses, was produced as a major product.[7] In the saccharide primer method, the fluorous tag does not inhibit regio- and stereo-specific glycosylation. Herein, we describe the immobilization of fluorous-tagged GM3-type oligosaccharide, obtained from animal cells, on commercially available polytetrafluoroethylene (PTFE) filter in order to develop a virus capture filter. This filter was used to screen the interaction between complex carbohydrates and either lectins or influenza virus.

In pursuit of the suitable molecular design for immobilization on the PTFE filter, we have synthesized lactose derivatives with various fluorous tags and assessed using the lactose-ECA (*Erythrina cristagalli agglutinin*) lectin interaction. Lactose derivatives, which were prepared from lactosyl imidate and corresponding alcohol, have different lengths of PEG-chain, as spacer, and a fluorous tag ($C_8F_{17}$) to enable the site specific immobilization of the compounds onto PTFE filter.[8] These compounds arrayed on the PTFE filter. The filters were dried, blocked by BSA, and then incubated with biotin-labeled ECA lectin. After washing with PBS buffer, the blots were incubated with avidin-labeled HRP. Then, the membranes were washed with PBS buffer, and ECL was detected. Positive interactions between lactose derivatives with PEG-chain as a spacer (Lac-PEG5-*F* **1** and Lac-PEG2-*F* **2**) and ECA were revealed (Fig. 1). In contrast, the lactose derivative without PEG-chain (Lac-*F* **3**) or the simple alcohol compound (HO-PEG2-*F* **4**) did not show carbohydrate–protein binding. Consequently, we found that the lactose derivative requires a spacer for the non-covalent carbohydrate immobilization on PTFE filter. Moreover, to confirm the

* Corresponding author.
*E-mail address:* mmizuno@noguchi.or.jp (M. Mizuno).

0960-894X/$ - see front matter © 2011 Elsevier Ltd. All rights reserved.
doi:10.1016/j.bmcl.2011.11.057

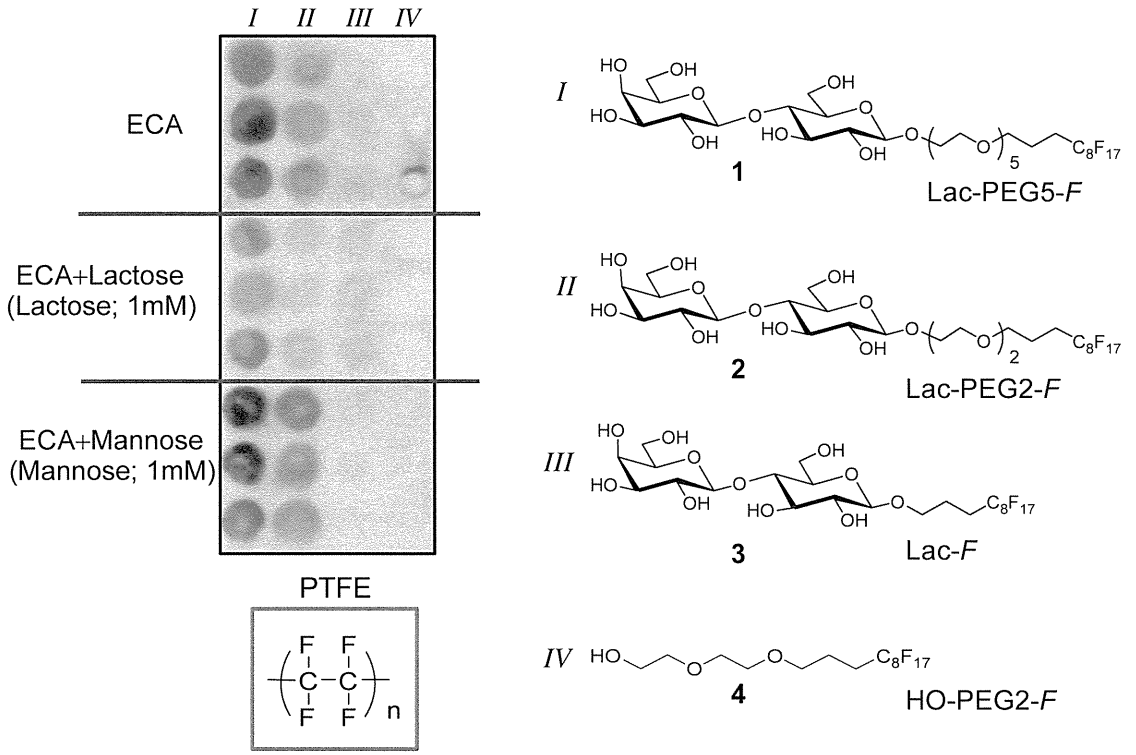


**Figure 1.** Detection and assessment of the carbohydrate–lectin interaction on a PTFE filter.

carbohydrate-binding specificity, ECA was incubated along with lactose or mannose as an competitor. Results showed that only lactose played a role as a competitor, indicating the carbohydrate-binding specificity of ECA.

To compare between PEG chain and alkyl chain as a spacer, we designed the oligosaccharides containing spacers with the similar total atom contents (Fig. 2). Detection of the lactose-ECA interaction indicated that ECA bound to the lactose derivative with PEG-chain (Lac-PEG2-*F* **2**) selectively. In contrast, the interaction of the alkyl chain (Lac-C10-*F* **5**) with ECA was negative. These results showed that a PEG-chain spacer was more suitable than an alkyl chain for the immobilization on the PTFE filter. The chemical nature of the spacer accounts for this difference. Since the PTFE filter repelled water, thus the ECA lectin in PBS buffer could not come near the PTFE filter. The highly hydrophilic nature of the PEG-chain helped lactose binding to the lectin in PBS buffer. On the other hand, the hydrophobicity of the alkyl chain avoided water. Thus, it is quite likely that the lactose with an alkyl chain on the PTFE filter did not bind to ECA lectin.

Based on these results, we carried out the immobilization of bio-active oligosaccharide on the PTFE filter. Lactoside primers with PEG5 and PEG2 (Lac-PEG5-*F* **1** and Lac-PEG2-*F* **2**, respectively) were introduced to mouse melanoma B16 cells (Scheme 1). The HPTLC results indicated that both PEG-fluorous primers were sialylated (Fig. 3). Moreover, the results showed that the lactoside primer with PEG2 was a more effective primer than that with a PEG5

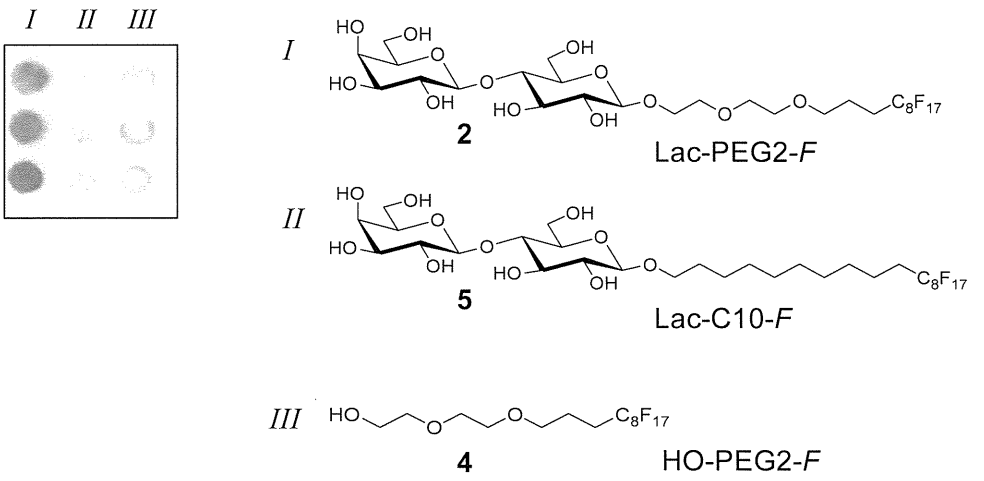


**Figure 2.** Comparison between PEG chain and alkyl chain as a spacer.

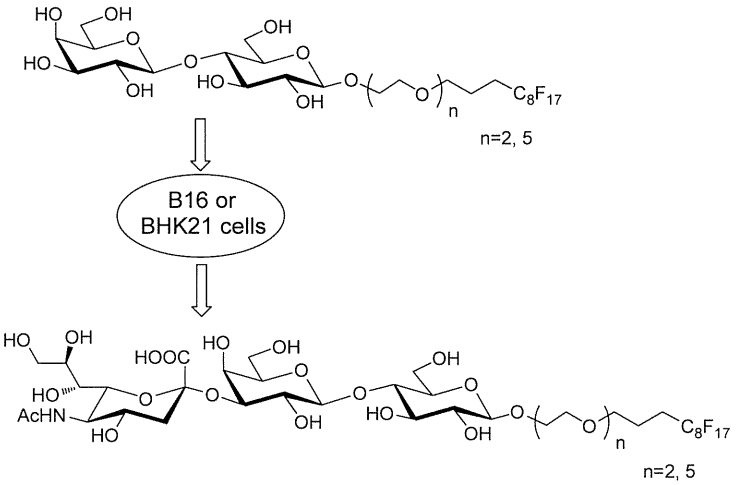


**Scheme 1.** Synthesis of GM3-type oligosaccharide using lactose primer and animal cells.

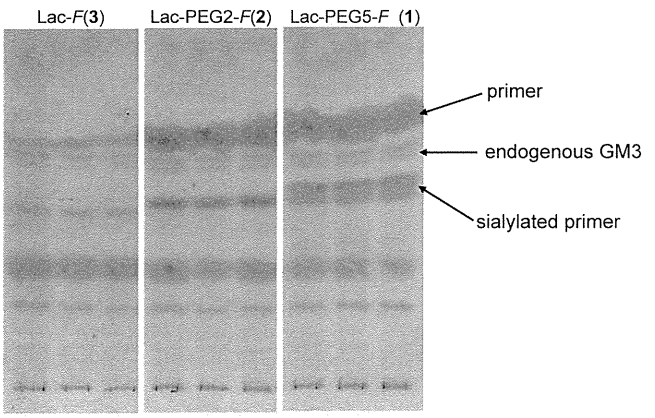


**Figure 3.** To verify, B16 cells ($2 \times 10^6$, 100 mm dish) were incubated for 48 h in the presence of 50 μM of Lac-PEG5-*F* (**1**), Lac-PEG2-*F* (**2**), Lac-*F* (**3**) primer (7 mL) in serum free 1:1 DMEM-F12 supplemented with transferrin and insulin. The culture media were collected and the lipids were extracted by Sep-Pak (C-18).

for sialylation. Recently, it was found that sialylation of normal alkyl saccharide primer was more efficient in BHK-21(C-13) cells than B-16 cells.[9] Hence, the primer was administered to BHK-21(C-13) cells. The lactoside primer was sialyated by BHK-21(C-13) cells to afford a GM3-type oligosaccharide as a major product. When administered to mouse melanoma B16 cells, we failed to isolate the sialylated products by fluorous silica gel. In spite of the presence of the fluorous tag, the compound eluted along with the non-fluorous compounds (elution 30% MeOH aq) because of the high polarity of the GM3-type oligosaccharide **6**. Therefore, purification was carried out as follows: (i) loading of cell culture medium on HP-20, (ii) washing with water, (iii) washing with 30% MeOH aq, (iv) elution with MeOH, (v) removal of MeOH, (vi) direct isolation by flash chromatography on silica gel.

The obtained GM3-type oligosaccharide **6** was immobilized on PTFE filter and the carbohydrate–lectin interaction was assayed. In this case, the compounds were easily arrayed onto the PTFE filter and then assayed using biotin labeled MAM (*Maackia amurensis*) and ECA lectin (Fig. 4). The obtained GM3-type oligosaccharide **6** selectively bound to MAM lectin. On the other hand, ECA bound to lactose derivative selectively. The result suggested that not only

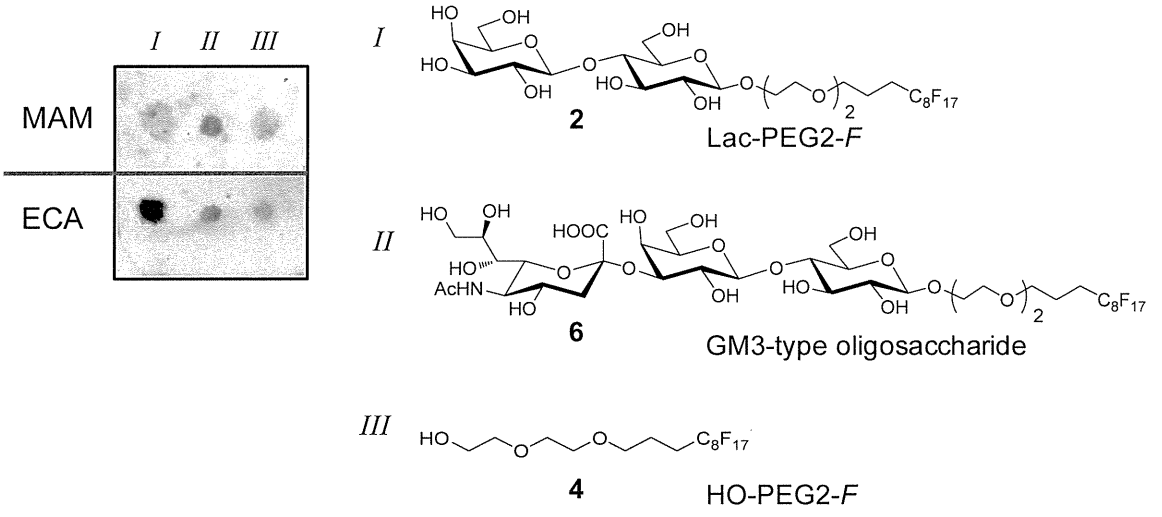


**Figure 4.** Screening of carbohydrate–lectin interaction by dot-blot.

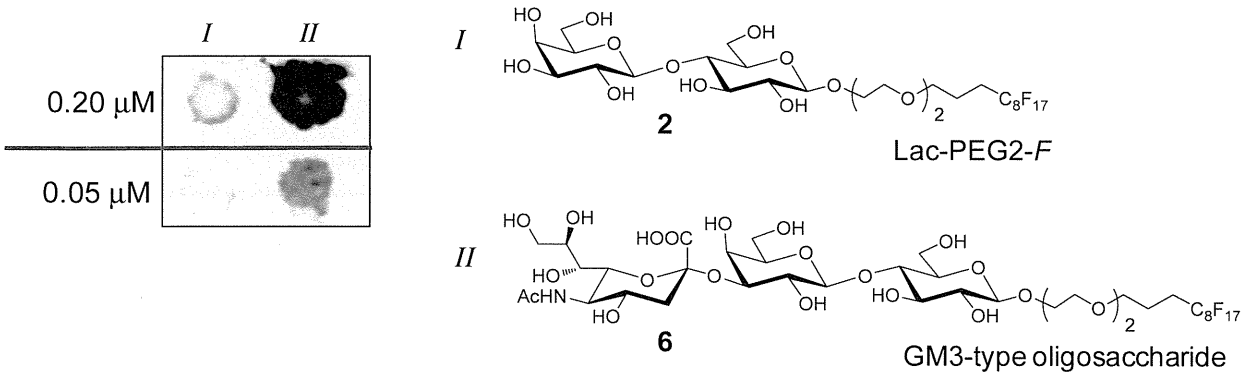


**Figure 5.** Detection and assessment of the interaction between carbohydrate derivatives and influenza A virus (strain A/duck/Pennsylvania/10218/84).

normal carbohydrate but also highly polar compounds such as the trisaccharide containing a sialic acid could be immobilized by non-covalent fluorous interaction on PTFE filter.

In addition, it was known that GM3-type oligosaccharide containing the α2,3 linkage to galactose binds to the hemagglutinin from avian isolates.[7] The satisfactory result for the assay between the obtained GM3-type oligosaccharide **6** and H5 influenza A virus hemagglutinin protein instead of lectin was obtained.[10]

Finally, the GM3-type oligosaccharide-influenza virus interaction was assayed. GM3-type oligosaccharide **6** arrayed on PTFE filter was assessed using Influenza A virus (strain A/duck/Pennsylvania/10218/84) as described above (Fig. 5). The influenza virus interacted selectively with the GM3-type oligosaccharide **6** in a dose-dependent manner. This satisfactory result suggested that the carbohydrate-binding specificity could be used for the detection of influenza virus.

In conclusion, carbohydrates with PEG-fluorous tag could be immobilized onto PTFE filter by spotting. The complex carbohydrate was easily prepared by using lactose primer with PEG-fluorous tag and BHK-21(C-13) cells and isolated by flash chromatography on silica gel. We confirmed that a PEG chain was better than an alkyl chain for the immobilization of saccharides on the PTFE filter. Significantly, the immobilization of a highly polar sialic acid-modified trisaccharide on the PTFE filter was achieved, and the interaction between carbohydrate and -proteins, which recognize sialic acid such as influenza virus hemmagglutinin, could be easily assessed.

## Acknowledgments

This work was supported by a Grant for 'Development of Novel Diagnostic and Medical Applications through Elucidation of Sugar Chain Functions, from New Energy and Industrial Technology Development Organization (NEDO).

## Supplementary data

Supplementary data associated with this article can be found, in the online version, at doi:10.1016/j.bmcl.2011.11.057.

## References and notes

1. For reviews see: (a) Studer, A.; Hadida, S.; Ferritto, R.; Kim, S.-Y.; Jeger, P.; Wipf, P.; Curran, D. P. *Science* **1997**, *275*, 823; (b) Curran, D. P. In *The Handbook of Fluorous Chemistry.*; (c)*Handbook of Fluorous Chemistry*; Gladysz, J. A., Curran, D. P., Horvath, I. T., Eds.; Wiley-VCH: Weinheim, 2004; Vol. 104, p 2531; (d) Curran, D. P. *Aldrichimica Acta* **2006**, *39*, 3.
2. (a) Ko, K.-S.; Jaipuri, F. A.; Pohl, N. L. *J. Am. Chem. Soc.* **2005**, *127*, 13162; (b) Mamidyala, S. K.; Ko, K.-S.; Jaipuri, F. A.; Park, G.; Pohl, N. L. *J. Fluorine Chem.* **2006**, *127*, 571.
3. Nicholson, R. L.; Ladlow, M. L.; Spring, D. R. *Chem. Commun.* **2007**, 3906.
4. For reviews see: (a) Duffner, J. L.; Clemons, P. A.; Koehler, A. N. *Curr. Opin. Chem. Biol.* **2007**, *11*, 74; (b) He, X. G.; Gerona-Navarro, G.; Jaffrey, S. R. *J. Pharmacol. Exp. Ther.* **2005**, *313*, 1; (c) Uttamchandani, M.; Walsh, D. P.; Yao, S. Q.; Chang, Y.-T. *Curr. Opin. Chem. Biol.* **2005**, *9*, 4.
5. Kasuya, M. C.; Ito, A.; Hatanaka, K. *J. Fluorine Chem.* **2007**, *128*, 562.
6. (a) Sato, T.; Hatanaka, K.; Hashimoto, H.; Yamagata, T. *Trends Glycosci. Glycotechnol.* **2007**, *19*, 1; (b) Kasuya, M. C.; Wang, Z. L. X.; Lee, Y. C.; Mitsuki, M.; Nakajima, H.; Hatanaka, K.; Sato, T.; Hatanaka, K.; Yamagata, S. *Carbohydr. Res.* **2000**, *329*, 755; (c) Kato, T.; Miyagawa, A.; Kasuya, M. C.; Ito, A.; Hatanaka, K. *J. Chromatogr., A.* **2008**, *1178*, 154; (d) Miura, Y.; Yamagata, T. *Biochem. Biophys. Res. Commun.* **1997**, *241*, 698.
7. For example, see (a) Stevens, J.; Blixt, O.; Tumpey, T. M.; Taubenberger, J. K.; Paulson, J. C.; Wilson, I. A. *Science* **2006**, *312*, 404; (b) Subbarao, K.; Klimov, A.; Katz, J.; Regnery, H.; Lim, W.; Hall, H.; Bender, C.; Huang, J.; Hemphill, M.; Rowe, T.; Shaw, M.; Xu, X.; Fukuda, K.; Cox, N. *Science* **1998**, *279*, 393; (c) John, J.; Skehel, J. J.; Wiley, D. C. *Annu. Rev. Biochem* **2000**, *69*, 531; (d) Suzuki, Y. *Prog. Lipid Res.* **1994**, *33*, 429.
8. See Supplementary data.
9. Unpublished data.
10. See Supplementary data for experimental data in detail.

Biochimica et Biophysica Acta 1820 (2012) 90–95

Contents lists available at SciVerse ScienceDirect

Biochimica et Biophysica Acta

journal homepage: www.elsevier.com/locate/bbagen

# Structure-based discovery of anti-influenza virus A compounds among medicines

Mayuko Fukuoka [a,b], Moeko Minakuchi [c], Atsushi Kawaguchi [c], Kyosuke Nagata [c], Yuji O. Kamatari [d], Kazuo Kuwata [a,b,*]

[a] United Graduate School of Drug Discovery and Medical Information Sciences, Gifu University, 1-1Yanagido, Gifu 501-1193, Japan
[b] CREST, Japan Science and Technology Agency, 4-1-8 Honcho, Kawaguchi, Saitama 332-0012, Japan
[c] Department of Infection Biology, Graduate School of Comprehensive Human Sciences, University of Tsukuba, 1-1-1 Tennodai, Tsukuba, 305-8575, Japan
[d] Life Science Research Center, Gifu University, 1-1 Yanagido, Gifu, 501-1194, Japan

ARTICLE INFO

*Article history:*
Received 19 August 2011
Received in revised form 4 November 2011
Accepted 7 November 2011
Available online 11 November 2011

*Keywords:*
Structure-based drug design
Influenza A virus
H1N1
RNA polymerase
PA
Surface plasmon resonance

ABSTRACT

*Background:* Influenza A virus (IAV) infection is nowadays a major public health concern, in particular since the 2009 H1N1 flu pandemic. The outbreak of IAV strains resistant to currently available drugs, such as oseltamivir or zanamivir targeting the neuraminidase, is a real threat for humans as well as for animals. Thus the development of anti-IAV drugs with a novel action mechanism may be an urgent theme.
*Methods:* We performed a docking simulation targeting the interface of PA interacting with PB1 using a drug database including ~4000 compounds. We then conducted cell viability assay and plaque assay using IAV/WSN/33. Finally we examined their anti-IAV mechanism by surface plasmon resonance and IAV replicon assay.
*Results:* We found that benzbromarone, diclazuril, and trenbolone acetate had strong anti-IAV activities. We confirmed that benzbromarone and diclazuril bound with PA subunit, and decreased the transcriptional activity of the viral RNA polymerase.
*Conclusions:* Benzbromarone and diclazuril had strong anti-IAV activities with novel action mechanism, i.e. inhibition of viral RNA polymerase.
*General significance:* Since benzbromarone and diclazuril are already used in public as medicines, these could be the candidates for alternatives in case of an outbreak of IAV which is resistant to pre-existing anti-IAV drugs.



## 1. Introduction

Influenza A virus (IAV) infection is nowadays a major public health concern, in particular since the 2009 H1N1 flu pandemic [1]. The outbreak of strains resistant to currently available drugs, such as oseltamivir and/or zanamivir which inhibit neuraminidase activity on the viral surface, is a real threat for humans as well as for animals [2–4]. Thus, the development of anti-IAV drugs with a novel action mechanism targeting proteins other than neuraminidase may be an urgent theme [5]. Several reports were already published on the discoveries of such novel anti-IAV compounds [6–8]. However, in general, it will take many years for new compounds to be examined for regulatory affairs, quality assurance and GMP/GLP/GCP compliance, and approved as drugs by governmental regulatory agencies. To meet these conflicting demands, i.e., novel mechanisms (targets) and needs for urgent usage as drugs, here we tried to discover compounds with anti-IAV activities among medicines which were already approved for the treatment of other diseases.

We targeted the interface of PA interacting with the N-terminal region of PB1 [9], both of which are subunits of the RNA polymerase in IAV, because its amino acid sequence was proven to be well-conserved among strains [9] and in particular, PA-binding domain of the polymerase subunit PB1 is highly conserved [10,11], which is crucial because our drugs somewhat mimic PA-binding domain of PB1. Practically, it is also important that the three-dimensional structure of PA subunit was already elucidated (PDB ID: 2ZNL) [9].

For *in silico* screening, we employed a software, ICM [12] and a drug database. Initially, we extracted 40 compounds based on the docking energy and the binding modes that were calculated by the ICM software [12]. At the current stage, the hit rate of *in silico* screening is known to be 2%-3% [13,14] and is usually more than ten times higher than that of random screening [15,16]. Therefore if we select 30–50 compounds, we may have a chance to find out at least one compound with anti-IAV activity among medicines.

We then examined the anti-IAV activities of the compounds using the WST-8 and the plaque assay against IAV A/WSN/33 (H1N1). We ultimately examined whether compounds chosen after a final round of selection possessed a binding affinity to PA subunit as well as an

* Corresponding author at: United Graduate School of Drug Discovery and Medical Information Sciences, Gifu University, 1-1Yanagido, Gifu 501-1193, Japan. Tel.: +81 58 230 6143; fax: +81 58 230 6144.
*E-mail address:* kuwata@gifu-u.ac.jp (K. Kuwata).

0304-4165/$ – see front matter © 2011 Elsevier B.V. All rights reserved.
doi:10.1016/j.bbagen.2011.11.003

inhibitory effect on viral RNA polymerase activities using 293T cells transfected with expression plasmids for viral RNA polymerase proteins and nucleoprotein (NP) required for the viral replicon assay [9,17]. We also discuss the practical usage of the newly discovered compounds and also their possible side effects.

## 2. Materials and methods

### 2.1. In silico screening

For docking simulation, we used the ICM simulation software [18]. PA structure was extracted from crystal structure of PA-PB1 complex from influenza virus RNA polymerase (PDB ID: 2ZNL) [9]. We used a database, Drug Database (GVK Bioscience, India) containing 4062 drugs which are currently used in public.

### 2.2. Compounds

Piroxicam (Wako Pure Chemicals, Osaka, Japan), rofecoxib (Kemprotec Limited, Middlesbrough, UK), tyropanoate sodium (Kemprotec), benzbromarone (Kemprotec), diclazuril (LKT Laboratories, Inc., Minnesota, USA), levothyroxine sodium (United States Pharmacopeia, Maryland, USA), trenbolone acetate (Wako), and ribavirin (Duchefa Biochemie, Haarlem, the Netherlands) were purchased and dissolved in DMSO at a concentration of 10 μM. In *ex vivo* experiments, the compounds were serially diluted with the experimental media.

### 2.3. Recombinant influenza PA subunit (239–716)

The recombinant protein PA subunit (239–716) from influenza A/Puerto Rico/8/1934 H1N1 [9] was a kind gift from Professor Sam-Yong Park at Yokohama City University.

### 2.4. Cells and viruses

Madin–Darby canine kidney cells (MDCK cells) were provided by Professor Hideto Fukushi, United Graduated School of Veterinary Sciences, Gifu University. MDCK cells were maintained in minimal essential medium (MEMα) (Wako) supplemented with 10% fetal bovine serum, penicillin (60 U/ml), and streptomycin (60 μg/ml) (Gibco) at 37 °C in an atmosphere of 5% $CO_2$. The influenza A virus strain A/WSN/33 (H1N1) was provided by Professor Yoshihiro Kawaoka, the Institute of Medical Science, the University of Tokyo.

### 2.5. WST-8 assay

We examined the anti-IAV activities of the compounds using the WST-8 assay and the influenza virus A/WSN/33. MDCK cells ($2\times10^5$ cells/well) were seeded in a 96-well plate and pre-cultured for 24 h. Cells were washed with serum-free MEMα, and infected with the A/WSN/33 virus (300 PFU) in MEMα supplemented with 1 mg/ml bovine serum albumin (Sigma) and 6 μg/ml trypsin (Difco) in the presence of each compound. At 48 h after infection, cells were washed and cell viability was measured using the Cell Counting Kit-8 (Dojindo, Japan). DMSO was used as a control and ribavirin as a positive control.

### 2.6. Plaque assay

A monolayer of MDCK cells in a 6-well plate was washed with serum-free MEMα, and the influenza virus was adsorbed onto the cells for 1 h. The cells were washed and overlaid with MEM 2× (Gibco) supplemented with 1 mg/ml BSA, 6 μg/ml trypsin, non-essential amino acids solution (Gibco) and 1% low-melting-temperature agarose, INA-Agar BA-30 (Funakoshi, Japan). Plaques were counted after 2 days of incubation.

### 2.7. Surface plasmon resonance (SPR) measurements

Interactions between the *influenza* PA subunit (239–716) and the compounds were analyzed using the BIAcore T200 system (GE Healthcare, Buckinghamshire, UK). PA subunit (239–716) was immobilized on a sensor chip (CM5) using an amine coupling kit (GE Healthcare, Buckinghamshire, UK). Various concentrations of compounds were injected into a running buffer (0.01 M HEPES pH7.4 containing 0.15 M NaCl, 0.1% surfactant P20, and 5% dimethyl sulfoxide (DMSO)) for 2 min at a flow rate of 30 μl/min at 10 °C. Then the running buffer without compounds was injected for 20 min at the same flow rate. Data were corrected using a blank sensor chip as a control. The dissociation constant ($K_D$) was calculated from the analyte (compound) concentration dependence of the sensorgram responses at equilibrium.

For curve fitting, we assumed the 1:1 binding model: $K_D = C(Rmax - R)/R$, where $K_D$, C, R and Rmax are dissociation constant, compound concentration, SPR response (r.u.; response unit) at the given compound concentration, and the maximum SPR response. Rmax is expected to be smaller than the theoretical maximum SPR response estimated from the response of immobilization, which was 12,782 r.u. for PA subunit.

### 2.8. Transcription assay

Human embryo kidney 293T cells ($2\times10^5$ cells/well) were cultured in a 12-well plate and transfected with the viral protein expression plasmids pcDNA-PA, pcDNA-PB1, pcDNA-PB2, and pCAGGS-NP, and the model viral gene expression plasmid pHH21-vNS-Luc using GeneJuice® (Novagene). We also transfected the Renilla luciferase expression plasmid pβ-Ruc GFP to be used as a control of transfection efficiency; this plasmid was transcribed by the cellular RNA polymerase II (Pol II). At 8 hours after transfection, the compounds serially diluted in DMSO (5 μM, 15 μM, 50 μM) were added. The cell lysates were harvested after 10 h of incubation and subjected to a luciferase assay [19] with the luciferase assay system (Promega). We measured the transcriptional activity of the influenza virus RNA polymerase by firefly luciferase activity and pβ-Ruc GFP by Renilla luciferase activity. The amount of proteins in all samples used for the luciferase assay was measured by the Bradford method [7].

## 3. Results

### 3.1. In silico docking simulation

We performed a docking simulation, targeting the binding site of PA with PB1 (PDB ID: 2ZNL) [9], using the program ICM and the Drug Database. According to the docking score, representing the free energy of binding and the visual confirmation of the docking modes, we initially selected 40 compounds which can be purchased from vendors. In Fig. 1, chemical structures, binding energies, and binding modes are depicted for three representative compounds, (A) benzbromarone, (B) diclazuril, and (C) trenbolone acetate. Their binding scores, representing the binding free energies, were −25.46, −25.93 and −26.12, respectively. These compounds are well-placed in the pocket constructed by the α10, α4, α13, α8, and α9 segments in PA [9], as shown in Fig. 1.

### 3.2. WST-8 and plaque assay

Cell viability and toxicity were assayed for 40 compounds at a concentration of 100 μM using the WST-8 assay. Many compounds showed no effects or in the same level as that of DMSO (the solvent used to dissolve the compounds), but seven compounds i.e. piroxicam (M.W. 331.35), rofecoxib (314.36), tyropanoate sodium (663.00), benzbromarone (424.08), diclazuril (407.64), levothyroxine sodium (816.87), and trenbolone acetate (270.37). We next conducted

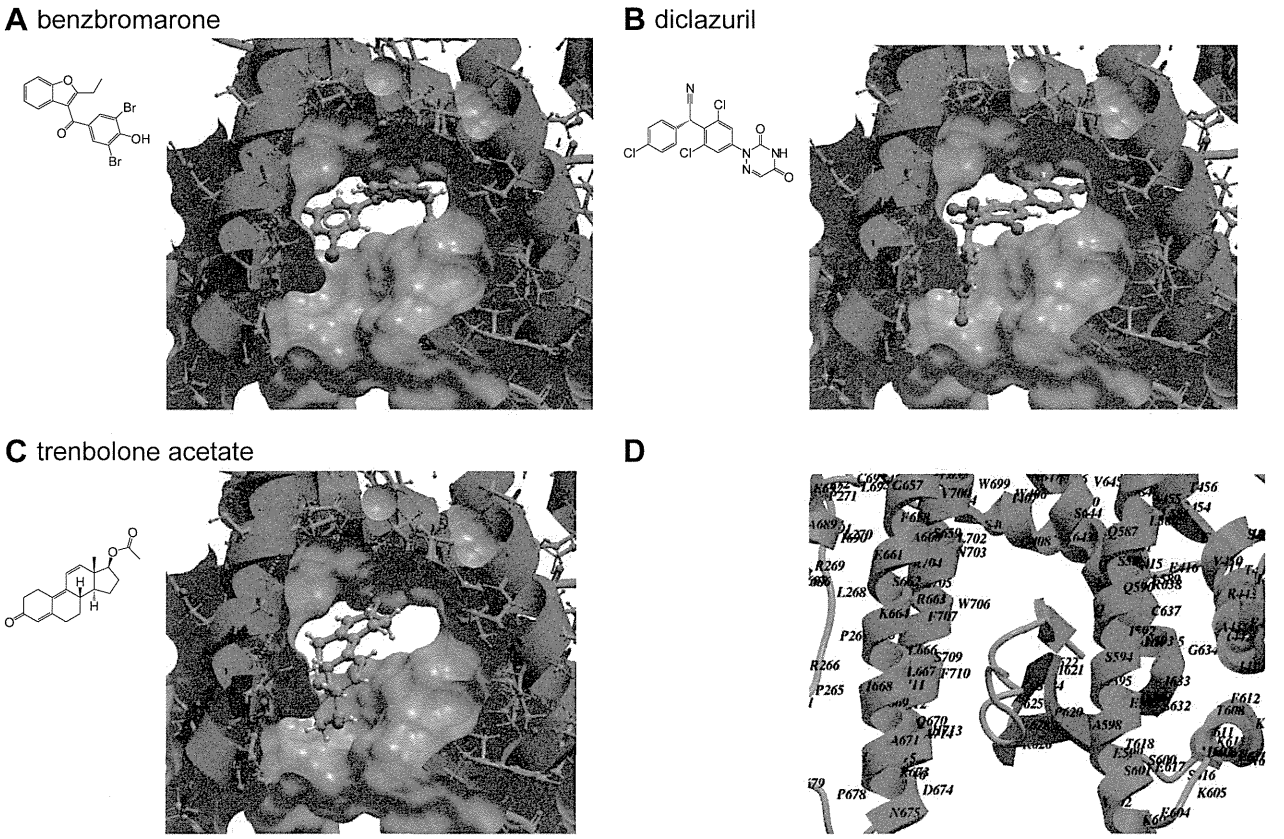


**Fig. 1.** Chemical formulae of drugs and their binding modes with PA, which is extracted from crystal structure of PA-PB1 complex from influenza virus RNA polymerase (PDB ID: 2ZNL) [9], obtained by the docking simulation using ICM. Compounds are colored in red. (A) benzbromarone; MW 424.08; calculated score −25.46. (B) diclazuril; MW 407.64; score −25.93. (C) trenbolone acetate; MW 270.37; score −26.12. (D) Binding region of PA with PB1 from crystal structure of PA-PB1 complex (PDB ID: 2ZNL) [9]. The PB1 and β8 segments in PA are colored in orange and blue, respectively.

plaque assays for seven compounds, and finally confirmed that benzbromarone, diclazuril, and trenbolone acetate had strong anti-virus activities. In order to determine the strength of the anti-virus activities for benzbromarone, diclazuril, and trenbolone acetate, we conducted plaque assays as a function of compound concentration, as shown in Fig. 2A, B, and C, respectively. Their $EC_{50}$ values were $39 \pm 1.7$, $31 \pm 5.3$, and $51 \pm 2.8$ μM, respectively, which were obtained by the curve fitting shown in Fig. 2D, E, and F, respectively.

### 3.3. SPR measurements

We estimated the dissociation constants ($K_D$) of compounds with PA subunit [9] using SPR. Assuming a 1:1 binding model, $K_D$ values were estimated to be 48.2, 211, and 91 μM for benzbromarone, diclazuril, and trenbolone acetate, respectively, as shown in Fig. 3. For benzbromarone, as shown in Fig. 3D, fitted curve clearly indicates a saturation at higher concentration of compound, and Rmax was calculated to be 80.3 r.u. (theoretical maximum value is 73.0 r.u.), suggesting the specific interaction with PA. Although we could estimate $K_D$ for diclazuril with large standard error, as shown in Fig. 3E, SPR response seemed to be almost linear as a function of compound concentrations suggesting the nonspecific character, and Rmax obtained from the initial four data points (288 r.u.) to reduce the contribution of the non-specific interaction was still larger than the theoretically expected maximum value, 95.3 r.u., which is inconsistent with a 1:1 binding model. In contrast, although the apparent $K_D$ for trenbolone was better than that of diclazuril, its Rmax was rather low (5.9 r.u.), as shown in Fig. 3F, indicating the essentially weak binding character.

### 3.4. Transcription assay

Next, we tested their effects on the transcriptional activities of the viral RNA polymerase with a viral replicon assay using 293T cells transfected with viral RNA polymerase protein expression plasmids and a plasmid expressing a reporter viral genome encoding the luciferase.

In Fig. 4, firefly luciferase activities normalized to Renilla luciferase activities are plotted as a function of different concentrations of seven compounds. Benzbromarone and diclazuril decreased the transcriptional activity of the viral RNA polymerase but trenbolone acetate was ineffective in this assay system. The principle of our assay system is schematically illustrated in Fig. 5.

## 4. Discussion

Although various tools are currently available for drug discovery [20], we employed the *in silico* screening because of its relatively higher hit rate [13,14] than the random screening [15,16]. Also we used ICM [12] because its performance and convenient usages were demonstrated already [13]. For target region, we selected the interface of PA interacting with the N-terminal region of PB1 extracted from crystal structure of PA-PB1 complex from influenza virus RNA polymerase (PDB ID: 2ZNL) [9]. The calculated scores shown in Fig. 1 roughly represent the free energy of binding between PA and compounds. These values (−25 to −27 kcal/mol) were slightly higher than −32 which is an empirical criterion for judging that compound could be a potential ligand. Scores around −32 could be attained when we used a larger database such as ACD (available compound directory) which includes approximately 8 million compounds

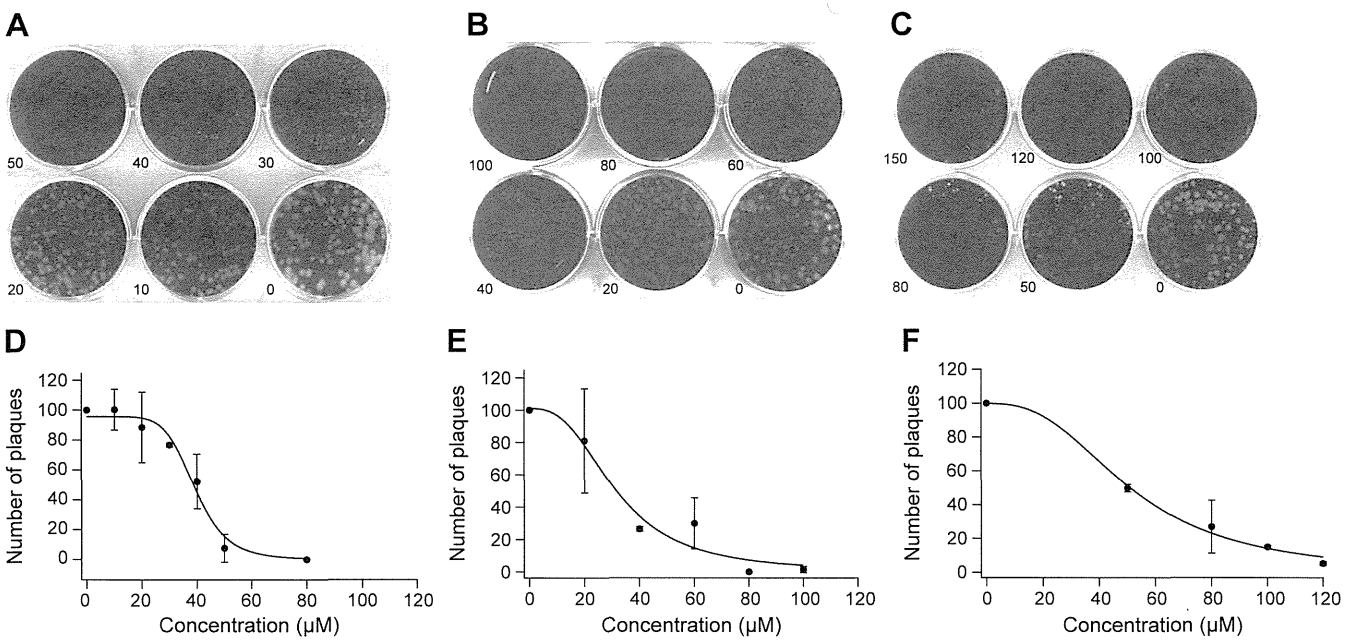


**Fig. 2.** Plaque inhibition assay for (A) benzbromarone, (B) diclazuril, and (C) trenbolone acetate. A monolayers of MDCK cells infected with influenza A virus were incubated for 2 days in the medium in which the serially diluted compound (10 to 150 μM) was added. The numbers of plaques are counted for (D) benzbromarone, (E) diclazuril, and (F) trenbolone acetate as a function of compound concentration, and their $EC_{50}$ values were estimated to be 39 ± 1.7, 31 ± 5.3, and 51 ± 2.8 μM, respectively.

[13]. Higher scores obtained here might be due to a rather limited number (4062) of compounds in the utilized database, and thus the optimum chemical structure for the target cavity might be incompletely explored. It should be noted that no explicit common scaffold was observed between hit compounds that demonstrated IAV activity, as shown in Fig. 1. This was also the case for the *in silico* docking simulation for prion diseases [14]. This can be explained either by the essentially weak binding properties of hit compounds, the lack of a unique scaffold for a particular cavity on a protein surface, or limited numbers of compounds in the utilized database. Previous research has shown that the hit rates of structure-based discovery are distributed from 1% to 5% [21–24]. Here the hit rate was 5% (2/40),

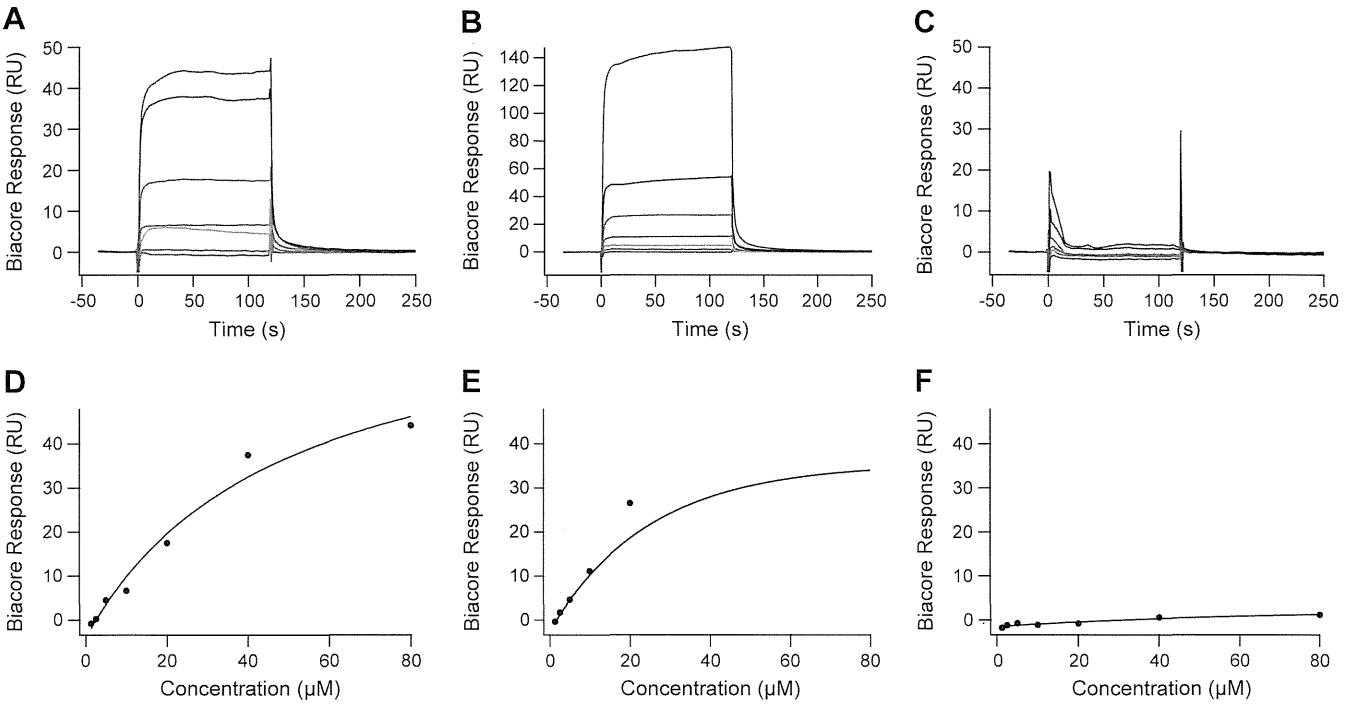


**Fig. 3.** Responses of surface plasmon resonance for the binding of (A) benzbromarone, (B) diclazuril, and (C) trenbolone acetate to the PA subunit (293–716) immobilized at 12,782 r.u. Brown, purple, blue, green, yellow, orange and red lines indicate the SPR responses to the compounds with concentrations of 80, 40, 20, 10, 5, 2.5 and 1.25 μM, respectively. Fitting curves are also shown for (E) benzbromarone, (F) diclazuril, and (G) trenbolone acetate. Assuming a 1:1 binding model, ($K_D$ ± S.E. (μM), Rmax ± S.E. (r.u.)) values were estimated to be (48.2 ± 23, 80.3 ± 15), (211 ± 760, 288 ± 980; fitting of the initial four data points), and (90.7 ± 110, 5.9 ± 4.1), respectively.

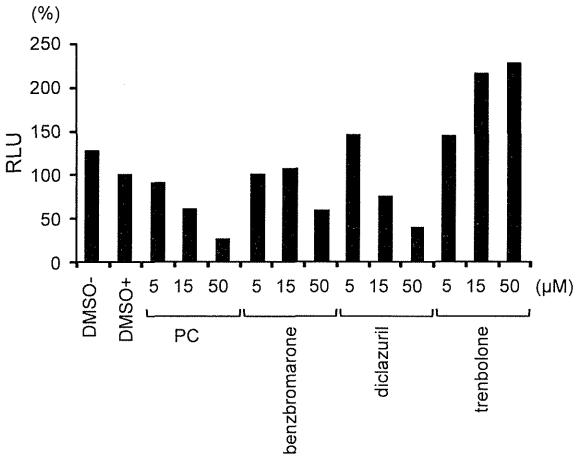


**Fig. 4.** Inhibitory effects on IAV polymerase transcriptional activity. HEK293T cells were transfected with viral protein expression plasmids and the standard Ruc-GFP expression plasmid. After incubation, serially diluted compounds (5, 15, 50 μM) were added. Luciferase activity was measured after 10 h. Transfectional activity of influenza virus RNA polymerase was measured by firefly luciferase activity. The ratio of DMSO (final concentration 0.5%) was set to 100%. All values were standardized by Renilla luciferase activity, thus representing the viral RNA polymerase activities.

and this value is relatively high among those reported previously. The reason may be that drugs are already in shapes that could easily function as ligands for proteins.

Firefly luciferase activities are essentially dependent on the cellular RNA polymerase I (Pol I) [25,26] activity to transcribe the negative-sense RNA from the vector DNA (pHH21-vNS-Luc) and also the Pol II activity to transcribe PB1, PB2, PA and NP mRNA from the vector DNAs (pcDNA-PB1, pcDNA-PB2, pcDNA-PA, pCAGGS-NP) as shown in Fig. 5. However, the Pol II activity was independently measured as the Renilla luciferase activity, which is dependent on the overall Pol II activity in the cell. Since the firefly luciferase activity was normalized to the Renilla luciferase activity, the Pol II activity dependency was essentially removed. The contribution of Pol I activity would be small because it would not be involved in the self-perpetuating replication process such as that carried out by viral RNA polymerase in this assay system. Therefore, the inhibitory effects of the compounds observed in Fig. 4 essentially would come from the direct inhibition of viral RNA polymerase.

Results of SPR measurements are consistent with those of the transcription assay. The interaction of benzbromarone with PA is relatively specific, while that of diclazuril is somewhat nonspecific. However, both inhibit the RNA polymerase activity because both bind to PA anyhow. On the other hand, since trenbolone interacts with PA rather weakly, it never inhibits the RNA polymerase activity (Fig. 4). Thus the observed anti-IAV activity of trenbolone may be attributed to the unknown mechanism other than binding to PA.

Obtained $K_D$ values of compounds are distributed between 48 and 211 μM, while that of wild type $PB1_{1-25}A$ peptides are ~1.8 nM [10]. When the same amounts of compounds and PB1 compete for binding to the cavity in PA, it would be disadvantageous to compounds. However, local concentration around the cavity of PA in the cell is also a crucial factor. When local concentration of compound is much higher than that of PB1, which consists of 757 amino acids, compounds could have a chance to interfere with the proper interaction between PA and PB1 by getting caught between them.

Although three anti-IAV compounds were successfully discovered among medicines, these also possess side effects, which are essentially dependent on dosage. Thus, it may be worthwhile to discuss their general usage and toxicity *in vivo*. Benzbromarone is a potent uricosuric agent, and has been used for the treatment of hyperuricemia and gout for approximately 30 years in many countries. Plasma concentrations at approximately 6 hours after a single oral dose (100 mg) of benzbromarone are roughly 10 μM [6]. Considering the $EC_{50}$ against the influenza A virus (~39 μM), benzbromarone may be a desirable alternative in case of an emergency, i.e., an outbreak of influenza A virus which is resistant to existent anti-IAV drugs, since its pharmacokinetics and pharmacodynamics are already clarified.

Diclazuril is characterized by its strong anti-coccidial activity and was developed as a commercial product in the late 1980s. Although it has been widely used for domestic animals, its application for human use has been limited to HIV infection. Toxicity for humans has not yet been completely established [7]. 80% of those orally treated with 1 mg/kg diclazuril were protected from acute toxoplasmosis [27]. Diclazuril had very low acute toxicity and was not mutagenic, genotoxic, carcinogenic, embryotoxic, fetotoxic, or teratogenic.

Trenbolone is an anabolic steroid used to promote growth in beef cattle. Immunochemistry experiments with the human androgen receptor (AR), as low as 1 pM, significantly induced androgen-dependent translocation of AR into the cell nucleus [28]. Trenbolone at doses of 0.5 mg/rat/day produced dose-dependent increases in the anogenital distance of female offspring at birth. Since trenbolone is known to induce developmental abnormalities in the fetus, a higher oral dose of trenbolone would be teratogenic. On the other hand, considering that methyltestosterone at a dose of 50 mg/day is usually administered for the treatment of male infertility in humans, temporal

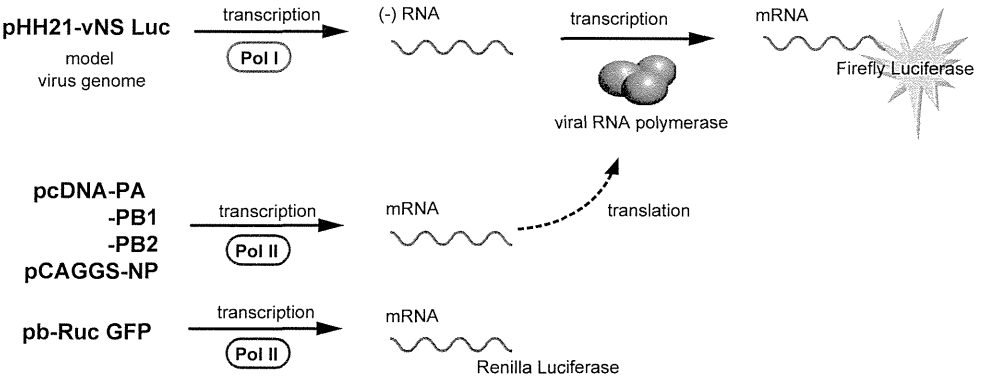


**Fig. 5.** Scheme of the utilized transcription assay system. Firefly luciferase activities are essentially dependent on Pol I activity to transcribe the negative-sense RNA from the vector DNA (pHH21-vNS-Luc) and also Pol II activity to transcribe the positive-sense PB1, PB2, PA, and NP mRNA from the vector DNA (pcDNA-PB1, pcDNA-PB2, pcDNA-PA, pCAGGS-NP). Pol II activity was independently measured by the Renilla luciferase activity, which is dependent on the overall Pol II activity in the cell.

administration of trenbolone for the treatment of viral infection would be acceptable, although further studies would be warranted.

In conclusion, initially we targeted PA and finally discovered the anti-IAV compounds diclazuril and benzbromarone, both of which possess inhibitory effects upon viral RNA polymerase, and trenbolone acetate whose anti-IAV mechanism is uncovered yet. Benzbromarone and diclazuril are already manufactured drugs and *in vivo* toxicities have already been investigated in detail. Moreover since they are currently utilized as medicines in public, they could be considered as candidates for alternative drugs in case of emergency, i.e., an outbreak of influenza A virus which is resistant to pre-existing anti-IAV drugs.

## Acknowledgements

We deeply thank Professor Sam-Yong Park for kindly providing with the recombinant protein PA (239–716). We thank Professor Hideto Fukushi for providing the MDCK cells and Professor Yoshihiro Kawaoka for providing the influenza A virus A/WSN/33 strain.

## References

[1] G. Neumann, T. Noda, Y. Kawaoka, Emergence and pandemic potential of swine-origin H1N1 influenza virus, Nature 459 (2009) 931–939.
[2] N.A.. Ilyushina, J.P. Seiler, J.E. Rehg, R.G.. Webster, E.A. Govorkova, Effect of neuraminidase inhibitor-resistant mutations on pathogenicity of clade 2.2 A/Turkey/15/06 (H5N1) influenza virus in ferrets, PLoS Pathog 6 (2010) e1000933.
[3] J. Longtin, S. Patel, A. Eshaghi, E. Lombos, R. Higgins, D. Alexander, R. Olsha, J. Doyle, D. Tran, A. Sarabia, C. Lee, N. Bastien, Y. Li, D. Low, G. Boivin, J. Gubbay, Neuraminidase-inhibitor resistance testing for pandemic influenza A (H1N1) 2009 in Ontario, Canada, J. Clin. Virol. 50 (2009) 257–261.
[4] F.G. Hayden, Antiviral resistance in influenza viruses—implications for management and pandemic response, N. Engl. J. Med. 354 (2006) 785–788.
[5] M. Kiso, K. Takahashi, Y. Sakai-Tagawa, K. Shinya, S. Sakabe, Q.M. Le, M. Ozawa, Y. Furuta, Y. Kawaoka, T-705 (favipiravir) activity against lethal H5N1 influenza A viruses, Proc. Natl. Acad. Sci. U. S. A. 107 (2010) 882–887.
[6] C.Y. Su, T.J. Cheng, M.I. Lin, S.Y. Wang, W.I. Huang, S.Y. Lin-Chu, Y.H. Chen, C.Y. Wu, M.M. Lai, W.C. Cheng, Y.T. Wu, M.D. Tsai, Y.S. Cheng, C.H. Wong, High-throughput identification of compounds targeting influenza RNA-dependent RNA polymerase activity, Proc Natl Acad Sci U S A 107 (2010) 19151–19156.
[7] I. Mickleburgh, F. Geng, L. Tiley, Mesoionic heterocyclic compounds as candidate messenger RNA cap analogue inhibitors of the influenza virus RNA polymerase cap-binding activity, Antivir. Chem. Chemother. 19 (2009) 213–218.
[8] W.L. Wang, D.Y. Yao, M. Gu, M.Z. Fan, J.Y. Li, Y.C. Xing, F.J. Nan, Synthesis and biological evaluation of novel bisheterocycle-containing compounds as potential anti-influenza virus agents, Bioorg. Med. Chem. Lett. 15 (2005) 5284–5287.
[9] E. Obayashi, H. Yoshida, F. Kawai, N. Shibayama, A. Kawaguchi, K. Nagata, J.R. Tame, S.Y. Park, The structural basis for an essential subunit interaction in influenza virus RNA polymerase, Nature 454 (2008) 1127–1131.
[10] K. Wunderlich, D. Mayer, C. Ranadheera, A.S. Holler, B. Manz, A. Martin, G. Chase, W. Tegge, R. Frank, U. Kessler, M. Schwemmle, Identification of a PA-binding peptide with inhibitory activity against influenza A and B virus replication, PLoS One 4 (2009) e7517.
[11] K. Wunderlich, M. Juozapaitis, C. Ranadheera, U. Kessler, A. Martin, J. Eisel, U. Beutling, R. Frank, M. Schwemmle, Identification of high-affinity PB1-derived peptides with enhanced affinity to the PA protein of influenza A virus polymerase, Antimicrob. Agents Chemother. 55 (2011) 696–702.
[12] C.N. Cavasotto, R.A. Abagyan, Protein flexibility in ligand docking and virtual screening to protein kinases, J. Mol. Biol. 337 (2004) 209–225.
[13] K. Kuwata, N. Nishida, T. Matsumoto, Y.O. Kamatari, J. Hosokawa-Muto, K. Kodama, H.K. Nakamura, K. Kimura, M. Kawasaki, Y. Takakura, S. Shirabe, J. Takata, Y. Kataoka, S. Katamine, Hot spots in prion protein for pathogenic conversion, Proc. Natl. Acad. Sci. U. S. A. 104 (2007) 11921–11926.
[14] J. Hosokawa-Muto, Y.O. Kamatari, H.K. Nakamura, K. Kuwata, Variety of antiprion compounds discovered through an in silico screen based on cellular-form prion protein structure: correlation between antiprion activity and binding affinity, Antimicrob. Agents Chemother. 53 (2009) 765–771.
[15] B.A. Posner, H. Xi, J.E. Mills, Enhanced HTS hit selection via a local hit rate analysis, J. Chem. Inf. Model. 49 (2009) 2202–2210.
[16] W. Zhou, P. Madrid, A. Fluitt, A. Stahl, X.S. Xie, Development and validation of a high-throughput screening assay for human long-chain fatty acid transport proteins 4 and 5, J. Biomol. Screen. 15 (2010) 488–497.
[17] K. Sugiyama, E. Obayashi, A. Kawaguchi, Y. Suzuki, J.R. Tame, K. Nagata, S.Y. Park, Structural insight into the essential PB1-PB2 subunit contact of the influenza virus RNA polymerase, EMBO J. 28 (2009) 1803–1811.
[18] C.N. Cavasotto, A.J. Orry, R.A. Abagyan, Structure-based identification of binding sites, native ligands and potential inhibitors for G-protein coupled receptors, Proteins 51 (2003) 423–433.
[19] Y.G. Chen, W.E. Kowtoniuk, I. Agarwal, Y. Shen, D.R. Liu, LC/MS analysis of cellular RNA reveals NAD-linked RNA, Nat. Chem. Biol. 5 (2009) 879–881.
[20] A. Smith, Screening for drug discovery: the leading question, Nature 418 (2002) 453–459.
[21] W.A. Lea, J. Xi, A. Jadhav, L. Lu, C.P. Austin, A. Simeonov, R.G. Eckenhoff, A high-throughput approach for identification of novel general anesthetics, PLoS One 4 (2009) e7150.
[22] F. El Turk, B. Fauvet, H. Ouertatani-Sakouhi, A. Lugari, S. Betzi, P. Roche, X. Morelli, H.A. Lashuel, An integrative in silico methodology for the identification of modulators of macrophage migration inhibitory factor (MIF) tautomerase activity, Bioorg. Med. Chem. 18 (2010) 5425–5440.
[23] O. Kalid, M. Mense, S. Fischman, A. Shitrit, H. Bihler, E. Ben-Zeev, N. Schutz, N. Pedemonte, P.J. Thomas, R.J. Bridges, D.R. Wetmore, Y. Marantz, H. Senderowitz, Small molecule correctors of F508del-CFTR discovered by structure-based virtual screening, J. Comput. Aided Mol. Des. 24 (2010) 971–991.
[24] Y. Chen, B.K. Shoichet, Molecular docking and ligand specificity in fragment-based inhibitor discovery, Nat. Chem. Biol. 5 (2009) 358–364.
[25] S.P. Bell, C.S. Pikaard, R.H. Reeder, R. Tjian, Molecular mechanisms governing species-specific transcription of ribosomal RNA, Cell 59 (1989) 489–497.
[26] P. Suphaphiphat, B. Keiner, H. Trusheim, S. Crotta, A.B. Tuccino, P. Zhang, P.R. Dormitzer, P.W. Mason, M. Franti, Human RNA polymerase I-driven reverse genetics for influenza a virus in canine cells, J. Virol. 84 (2010) 3721–3725.
[27] G. Sydow, V. Wunderlich, L. Baumbach, E. Tonew, M. Tonew, H.P. Schroer, The biological effects of coordination compounds of transitional metals. 6. Effect of 4-methyl-2-aminopyridine-palladium chloride and cis-dichlorodiammine-platinum(II) on retroviruses and the virus-associated RNA polymerase of the influenza virus, Zentralbl. Bakteriol. Mikrobiol. Hyg. A 262 (1986) 169–178.
[28] D. McGeoch, N. Kitron, Influenza virion RNA-dependent RNA polymerase: stimulation by guanosine and related compounds, J. Virol. 15 (1975) 686–695.

JVI
Journals.ASM.org

# Wild-Type Measles Virus with the Hemagglutinin Protein of the Edmonston Vaccine Strain Retains Wild-Type Tropism in Macaques

Kaoru Takeuchi,[a] Noriyo Nagata,[b] Sei-ich Kato,[a] Yasushi Ami,[c] Yuriko Suzaki,[c] Tadaki Suzuki,[b] Yuko Sato,[b] Yasuko Tsunetsugu-Yokota,[d] Kazuyasu Mori,[e] Nguyen Van Nguyen,[a] Hideki Kimura,[a] and Kyosuke Nagata[a]

Department of Infection Biology, Division of Biomedical Science, Faculty of Medicine, University of Tsukuba, Tsukuba,[a] and Department of Pathology,[b] Division of Animal Experiments,[c] Department of Immunology,[d] and AIDS Research Center,[e] National Institute of Infectious Diseases, Tokyo, Japan

**A major difference between vaccine and wild-type strains of measles virus (MV) *in vitro* is the wider cell specificity of vaccine strains, resulting from the receptor usage of the hemagglutinin (H) protein. Wild-type H proteins recognize the signaling lymphocyte activation molecule (SLAM) (CD150), which is expressed on certain cells of the immune system, whereas vaccine H proteins recognize CD46, which is ubiquitously expressed on all nucleated human and monkey cells, in addition to SLAM. To examine the effect of the H protein on the tropism and attenuation of MV, we generated enhanced green fluorescent protein (EGFP)-expressing recombinant wild-type MV strains bearing the Edmonston vaccine H protein (MV-EdH) and compared them to EGFP-expressing wild-type MV strains. *In vitro*, MV-EdH replicated in SLAM$^+$ as well as CD46$^+$ cells, including primary cell cultures from cynomolgus monkey tissues, whereas the wild-type MV replicated only in SLAM$^+$ cells. However, in macaques, both wild-type MV and MV-EdH strains infected lymphoid and respiratory organs, and widespread infection of MV-EdH was not observed. Flow cytometric analysis indicated that SLAM$^+$ lymphocyte cells were infected preferentially with both strains. Interestingly, EGFP expression of MV-EdH in tissues and lymphocytes was significantly weaker than that of the wild-type MV. Taken together, these results indicate that the CD46-binding activity of the vaccine H protein is important for determining the cell specificity of MV *in vitro* but not the tropism *in vivo*. They also suggest that the vaccine H protein attenuates MV growth *in vivo*.**

Measles remains a major cause of childhood morbidity and mortality worldwide especially in developing countries in spite of significant progress in global measles control programs. Measles virus (MV), belonging to the genus *Morbillivirus* of the family *Paramyxoviridae*, is an enveloped virus with a nonsegmented negative-strand RNA genome (11). The MV genome encodes 6 structural proteins: the nucleocapsid (N), phospho (P), matrix (M), fusion (F), hemagglutinin (H), and large (L) proteins. Two envelope glycoproteins, the F and H proteins, initiate infection of the target cells via binding of the H protein to its cellular receptors. Therefore, the H protein is of primary importance for determining the cell specificity of MV (22).

The Edmonston strain of MV was isolated in 1954 by using a primary culture of human kidney cells (7). The Edmonston strain was subsequently adapted in a variety of cells, including chicken embryo fibroblasts, to enable the production of attenuated live vaccines, which are currently used worldwide (27). These live, attenuated MV strains are safe and induce strong cellular and humoral immune responses against MV. The Edmonston vaccine strain is no longer pathogenic in monkey models (2, 7, 37, 39). In contrast, wild-type MV strains isolated and passaged in B95a cells induce clinical signs resembling those of human measles in experimentally infected cynomolgus and rhesus monkeys (15, 16).

A major difference between vaccine and MV wild-type strains *in vitro* is their cell specificity. Vaccine strains of MV grow efficiently in many human and primate cell lines, whereas wild-type strains of MV grow only in limited lymphoid cell lines. This difference is attributed mainly to the receptor usage of MV strains. The H proteins of wild-type strains recognize the signaling lymphocyte activation molecule (SLAM) (also called CD150), which is expressed in certain immune system cells (36), and the recently identified nectin-4 (also called PVRL4), which is expressed in epithelial cells in trachea, skin, lung, prostate, and stomach as a cellular receptor (20, 23). However, the H proteins of MV vaccine strains recognize CD46 (6, 21) in addition to SLAM and nectin-4 as cellular receptors. Since CD46 is expressed in all human and monkey nucleated cells, MV vaccine strains can grow in many human and primate cell lines. Indeed, when the H protein of a wild-type strain of MV was exchanged with that of an MV vaccine strain, the resulting recombinant wild-type MV strain grew in many human and monkey cell lines (12, 28, 35).

Although the receptor specificity of the H proteins of MV strains has been studied extensively, very little is known about the effect of the H protein on the *in vivo* tropism and attenuation of MV. Given that the H proteins of MV vaccine strains can use CD46 in addition to SLAM and nectin-4 as cellular receptors, recombinant MV strains bearing the H protein of MV vaccine strains may have an expanded *in vivo* tropism.

In this study, we generated enhanced green fluorescent protein (EGFP)-expressing recombinant wild-type strains of MV bearing the H protein of the Edmonston MV vaccine strain by using our reverse genetics system (32) and compared the cell specificity *in vitro* and tropism *in vivo* with those of EGFP-expressing MV wild-type strains. We found that the H protein of the Edmonston vaccine strain of MV alters the cell specificity of the MV wild-type strain *in vitro* but does not alter the tropism of the MV wild-type

Received 8 October 2011 Accepted 23 December 2011
Published ahead of print 11 January 2012
Address correspondence to Kaoru Takeuchi, ktakeuch@md.tsukuba.ac.jp.

doi:10.1128/JVI.06517-11

strain *in vivo*. Furthermore, the H protein of the Edmonston vaccine strain attenuates MV growth in macaques.

## MATERIALS AND METHODS

**Cells and viruses.** B95a cells (an adherent marmoset B-cell line transformed with Epstein-Barr virus) (15) were maintained in Dulbecco's modified essential medium (DMEM) supplemented with 10% fetal bovine serum (FBS). Chinese hamster ovary (CHO) cells constitutively expressing human SLAM (CHO/hSLAM) (29) were maintained in RPMI 1640 medium supplemented with 10% FBS and 500 $\mu$g of G418 per ml. Primary cynomolgus monkey astroglial cells were obtained from Nobuyuki Kimura (National Institute of Biomedical Innovation, Tsukuba, Japan). IC323-EGFP was obtained from Yusuke Yanagi (Kyushu University, Fukuoka, Japan) (12). Vaccinia virus vTF7-3 encoding T7 RNA polymerase was obtained from Bernard Moss (National Institutes of Health, Bethesda, MD) (9).

**Preparation of primary cynomolgus monkey kidney cells.** The kidneys of a cynomolgus monkey were removed, sliced into small pieces, and digested with 0.3% trypsin in Hanks' balanced salt solution (HBBS) at 37°C with continuous stirring for an appropriate period. The dispersed cells were collected and washed twice with HBBS. The cells were suspended in DMEM supplemented with 10% FBS, seeded on a plate, and incubated at 37°C. Cells that grew as a monolayer culture were passaged, and the cells at passages 3 to 5 were used in the experiments.

**Construction of full-length cDNAs and reverse genetics.** Plasmid p(+)MV323, carrying the full-genome cDNA of the IC-B strain, has been described previously (15, 32, 33). Plasmid p(+)MV017, carrying the full-genome cDNA of the IC-B strain containing the H gene of the Edmonston B strain (Z66517), has been described previously (35). To exchange the H gene of p(+)MV323-EGFP with that of the Ed strain, a PacI-SpeI fragment containing the H gene was excised from p(+)MV323-EGFP and replaced with the corresponding fragment from p(+)MV017, resulting in p(+)MV017-EGFP. To introduce the EGFP gene between the F and H genes of p(+)MV323 and p(+)MV017, the open reading frame of an enhanced green fluorescent protein (EGFP) gene was first amplified from pEGFP-N1 (Clontech, Mountain View, CA) by using the primers 5′-ATCAGGGACAAGAGCAGGATTAGGGATATCCGAGATGGTGAGCAAGGGCGAGGA-3′ and 5′-GATGTTGTTCTGGTCCTCGGCCTCTCGCACTTACTTGTACAGCTCGTCCA-3′ and then using the primers 5′-GCGTTAATTAAAACTTAGGATTCAAGATCCTATTATCAGGGACAAGAGCAGGAT-3′ and 5′-GCGTTAATTAACAATGATGGAGGGTAGGCGGATGTTGTTCTGGTCCTCGG-3′ to introduce a PacI recognition site (underlined). After digestion with PacI, the EGFP fragment was inserted into the PacI sites in p(+)MV323 and p(+)MV017, resulting in p(+)MV323-EGFP(F/H) and p(+)MV017-EGFP(F/H), respectively. Recombinant MV strains EdH-EGFP, IC323-EGFP$_2$ and EdH-EGFP$_2$ were generated from the p(+)MV017-EGFP, p(+)MV323-EGFP(F/H), and p(+)MV017-EGFP(F/H) plasmids, respectively, by using CHO/hSLAM cells and vaccinia virus vTF7-3 as reported previously (29). IC323-EGFP, EdH-EGFP, IC323-EGFP$_2$, and EdH-EGFP$_2$ were propagated in B95a cells, and virus stocks at 3 to 4 passages in B95a cells were used for experiments. The amino acid sequence of the F protein of the IC-B strains (NC_001498/AB016162) is identical to that of the F protein of the Edmonston-B strain (Z66517).

**Infection of cynomolgus monkeys with recombinant MVs.** Cynomolgus monkeys were inoculated intranasally with $10^5$ times the 50% tissue culture infective dose ($TCID_{50}$) of IC323-EGFP$_2$ or EdH-EGFP$_2$ by using a nasal spray (Keytron, Chiba, Japan). Three animals (no. 4848, 4849, and 4850) were juvenile (1 year old), and 6 animals (no. 5056, 5057, 5058, 5062, 5068, and 5069) were 4 to 5 years old. All animals were seronegative for MV. Peripheral blood mononuclear cells (PBMCs) were isolated using a Percoll gradient (Amersham, Piscataway, NJ) diluted with a 1.5 M NaCl solution to 1.07 g/ml. MV-infected cells in PBMCs, spleens, and cervical lymph nodes were counted as previously reported (32). All animal experiments were performed in compliance with the guidelines of National Institute of Infectious Disease (Tokyo, Japan).

**Macroscopic detection of EGFP fluorescence.** EGFP fluorescence in the tissues and organs of cynomolgus monkeys was observed using a VB-G25 fluorescence microscope equipped with a VB-7000/7010 charge-coupled device (CCD) detection system (Keyence, Osaka, Japan). For the respective excitation and the detection of fluorescence, 470/40-nm and 510-nm band-pass filters were used.

**Histopathological and immunohistochemical analysis.** Animals were anesthetized, and tissues from lung, bronchus, heart, liver, kidney, skin, spleen, mesenteric lymph node (MLN), cervical lymph node, thymus, salivary gland, tonsil, stomach, pancreas, and jejunum were fixed with 10% phosphate-buffered formalin. Fixed tissues were embedded in paraffin, sectioned, and stained with hematoxylin and eosin. Immunohistochemical detection of the N protein of MV was performed on paraffin-embedded sections as described previously (34).

**Double immunofluorescence staining.** Paraffin-embedded lungs were used for staining the N protein of MV and cytokeratin. The sections were subjected to a double immunofluorescence staining method employing a rabbit antiserum against the N protein and the cytokeratin monoclonal mouse antibody (clone MAB1611; Chemicon, CA). Briefly, after deparaffinization with xylene, the sections were rehydrated in ethanol and immersed in phosphate-buffered saline (PBS). Antigens were retrieved by hydrolytic autoclaving for 15 min at 121°C in the retrieval solution at pH 9.0 (Nichirei, Tokyo, Japan). After cooling, normal goat serum was used to block background staining. The sections were incubated with the anticytokeratin antibody for 30 min at 37°C. After 3 washes in PBS, the sections were incubated with an antiserum against MV N protein for 30 min at 37°C. Antigen-binding sites were detected with goat anti-rabbit Alexa Fluor 488 (Molecular Probes, Eugene, OR) or goat anti-mouse Alexa Fluor 546 (Molecular Probes) for 30 min at 37°C. The sections were mounted with SlowFade Gold antifade reagent with DAPI (4′,6′-diamidino-2-phenylindole) (Molecular Probes), and the images were captured using a fluorescence microscope (IX71; Olympus, Tokyo, Japan) equipped with a Hamamatsu high-resolution digital B/W CCD camera (ORCA2; Hamamatsu Photonics, Hamamatsu, Japan).

**Flow cytometric analysis.** PBMCs were stained with the following monoclonal antibodies, which are cross-reactive with macaque cells: CD150-phycoerythrin (PE) clone A12 (BD Pharmingen, San Diego, CA), CD3-allophycocyanin (APC) clone SP34-2 (BD Pharmingen), and CD20-PE/Cy7 clone 2H7 (BioLegend, San Diego, CA). The cells were fixed with 1% paraformaldehyde, and MV-infected cells were detected by the expression of EGFP in the fluorescein isothiocyanate channel. The flow cytometric acquisition of approximately 200,000 to 500,000 events from each sample was performed on a FACSCalibur instrument.

**Amplification of MV genomic RNA by real-time reverse transcription-PCR (RT-PCR).** Total RNA was isolated from tissues by using the RNAlater and RNeasy kit (Qiagen, Hilden, Germany) according to the manufacturer's protocol, reverse transcribed, and PCR amplified with a Dice TP800 thermal cycler (Takara, Tokyo, Japan) by using Fast-Start SYBR green Master (Roche). For amplification of the MV genome sequence, MV-P1 primer 5′-AGATGCTGACTCTATCATGG-3′ (positions 2178 to 2197) was used for RT, and then MV-P1 primer and MV-P2 primer 5′-TCGAGCACATTGGGTTGCAC-3′ (positions 2574 to 2555) were used for PCR. For amplification of the 18S RNA segment, the 18S sense primer TCAAGAACGAAAGTCGGAGG and 18S antisense primer GGACATCTAAGGGCATCACA (25) were used. In a separate experiment, we amplified DNA from a known amount of p(+)MV323-EGFP plasmid containing the target region under the same reaction conditions, and the results for the real-time RT-PCR were expressed as genome RNA equivalent to p(+)MV323-EGFP.

**Cytokine assay.** Cytokine levels in the plasma were measured with a Luminex 200 instrument (Luminex, Austin, TX) by using a Milliplex non-human primate cytokine/chemokine kit (Millipore, Billerica, MA) according to the manufacturer's instructions. The assay sensitivities were as